T.C.
DOKUZ EYLÜL UNIVERSITY
IZMIR INTERNATIONAL
BIOMEDICINE AND GENOME
INSTITUTE

# UNDERSTANDING THE MOLECULAR MECHANISMS INVOLVED IN BLADDER TUMORIGENESIS USING EXPERIMENTAL AND COMPUTATIONAL APPROACHES

ALEYNA ERAY

MOLECULAR BIOLOGY AND GENETICS
**MASTER'S THESIS**

**İZMİR-2021**

**THESIS ID:** DEU.IBG.MSc/2018850001

T.C.
DOKUZ EYLÜL UNIVERSITY
IZMIR INTERNATIONAL
BIOMEDICINE AND GENOME
INSTITUTE

# UNDERSTANDING THE MOLECULAR MECHANISMS INVOLVED IN BLADDER TUMORIGENESIS USING EXPERIMENTAL AND COMPUTATIONAL APPROACHES

MOLECULAR BIOLOGY AND GENETICS
**MASTER'S THESIS**

**ALEYNA ERAY**

ADVISOR: DOÇ.DR. GÖKHAN KARAKÜLAH
CO-ADVISOR: DR. SERAP ERKEK ÖZHAN

This study is supported by EMBO 4148

**THESIS ID:** DEU.IBG.MSc/2018850001

Dokuz Eylül Üniversitesi İzmir Uluslararası Biyotıp ve Genom Enstitüsü Moleküler Biyoteknoloji Anabilim Dalı,
Moleküler Biyoloji ve Genetik Yüksek Lisans programı öğrencisi Aleyna ERAY **'Mesane tümör oluşumunda görev alan moleküler mekanizmaların deneysel ve hesaplamalı yaklaşımlar ile anlaşılması'** konulu Yüksek Lisans tezini 25/08/2021 tarihinde başarılı olarak tamamlamıştır.

BAŞKAN

Doç. Dr. Gökhan KARAKÜLAH
Dokuz Eylül Üniversitesi

ÜYE

Doç. Dr. Şerif ŞENTÜRK
Dokuz Eylül Üniversitesi

ÜYE

Dr. Öğr. Üyesi Ayşe Banu DEMİR
İzmir Ekonomi Üniversitesi

YEDEK ÜYE
Dr. Öğr. Üyesi Yavuz Oktay
Dokuz Eylül Üniversitesi

YEDEK ÜYE
Dr. Öğr. Üyesi Cihangir Yandım
İzmir Ekonomi Üniversitesi

**TABLE OF CONTENTS**

## INDEX OF TABLES

## INDEX OF FIGURES

## ABBREVIATIONS

KDM6A: Lysine demetyhlase 6A

ChIP: Chromatin immunoprecipitation

H3K9me3: Histone 3 lysine 9 trimethylation

PRC2: Polycomb repressor complex 2

HAT: Histone acetyl transferase

HDAC: Histone deacetylase

H3K4me3: Histone 3 lysine 4 trimethylation

NSCLC: Non-small cell lung cancer

MIBC: Muscle invasive bladder cancer

NMIBC: Non-muscle invasive bladder cancer

BCG: Bacille Calmette-Guérin

MLL: Lysine methyltransferase

EZH2: Histone-Lysine N-Methyltransferase

FBS: Fatal Bovine Serum

PBS: Phosphate Buffered Saline

EMBL: European Molecular Biology Laboratories

RMA: Robust Multichip Average

QN: Quantile Normalization

TSS: Transcription start site

NE-like: Neuroendocrine like

## ACKNOWLEDGEMENTS

First and foremost, I would like to express my deepest gratitude to my advisor Dr. Serap ERKEK ÖZHAN for giving me the opportunity to carry out this project, for her invaluable guidance and help, and her endless faith in me. It was and always will be an honor and pleasure to study under her supervision.

I also would like to express my gratitude to my co-advisor Doç. Dr. Gökhan KARAKÜLAH for his precious advice, guidance, help, and mentorship throughout this thesis process.

I would like to thank my lab members and friends Gülden ÖZDEN YILMAZ, Perihan Yağmur GÜNERİ, Burcu AKMAN for their endless patience, help, and great friendships. I also owe a huge debt of gratitude to Aslı KORKMAZ, my colleague and housemate, for her unending patience, love, and support.

I would like to express my gratitude to Doç. Dr. Şerif ŞENTÜRK and his lab members for their expertise, patience, and help with my experiments.

I owe a great appreciation to IBG-BİP Bioinformatics Platform for their support and help with my computational analyses throughout my thesis studies.

I would like to thank to European Molecular Biology Organization (EMBO) for their financial support in carrying out this project (EMBO 4148).

Lastly, I would like to thank my mother Selda BAYSAL for her love, support, and faith in me from the very beginning of my journey, and also my father Mustafa ERAY for his support.

I would also like to thank my loved ones that I could not thank individually, for being with me and supporting me.

UNDERSTANDING THE MOLECULAR MECHANISMS INVOLVED IN BLADDER TUMORIGENESIS USING EXPERIMENTAL AND COMPUTATIONAL APPROACHES


## ABSTRACT

It is known that genes involved in chromatin regulation are highly mutated in bladder cancer. For this reason, it is very important to understand the molecular mechanisms that play a role in the epigenetic regulation of bladder cancer and that may cause tumor formation. The primary goal in this thesis is to decipher the epigenetic mechanisms deregulated in bladder cancer using both experimental and computational methods. For this aim, first regulatory landscapes of bladder cancer molecular subtypes have been investigated using published data which showed active chromatin regions in bladder cancer using ATAC-seq. Our results showed upregulation of ß-catenin targets regulated by neuronal regulatory elements in three different cohorts, implicating ß-catenin signature in neuronal bladder cancer. Further, integration with mutation data revealed significantly higher oncogenic exon 3 ß-catenin mutations in neuronal bladder cancer compared to non-neuronal. Secondly, we aimed to understand the epigenetic deregulation in bladder cancer via employing experimental techniques. For this purpose, we focused on KDM6A, which is among the top frequently mutated chromatin modifiers in bladder cancer. To investigate how KDM6A depletion affects phenotypic and epigenomic profile of bladder cancer, we knock-out KDM6A in a muscle invasive bladder cancer cell line, 5637. No significant viability changes between 5637 and KDM6A-null 5637 have been detected in long term growth of the cells. Genes marked with top H3K4me3 peaks were enriched for chromatin organization pathway, including the chromatin modifier, HDAC1. Our findings suggest that in the absence of KDM6A chromatin modifier, repressive chromatin states might be abundant, which will be further investigated in future.

MESANE TÜMÖR OLUŞUMUNDA GÖREV ALAN MOLEKÜLER MEKANIZMALARIN DENEYSEL VE HESAPLAMALI YAKLAŞIMLAR ILE ANLAŞILMASI


## ÖZET

Mesane kanserinde kromatin regülasyonunda görevli genlerin sıklıkla mutasyona uğradığı bilinmektedir. Bu sebeple mesane kanserinin epigenetik regülasyonunda rol oynayan ve tümör oluşumuna sebep olabilecek moleküler mekanizmaları anlamak oldukça önemlidir. Bu tez kapsamında öncelikli amaç, mesane kanserinde deregüle olan epigenetik mekanizmaların hem deneysel hem de hesaplamalı yöntemler kullanılarak anlaşılmasını sağlamaktır. Bu nedenle, ilk olarak, mesane kanseri alt tiplerinin düzenleyici kromatin bölgeleri üzerinde açık bölgelerdeki sinyallerin tespit edildiği güncel yayınlanmış ATAC-Seq verileri incelendi. Bulgular, nöronal mesane kanserinde üç farklı çalışma grubunda nöronal düzenleyici unsurlar tarafından düzenlenen ß-catenin hedef genlerinin artışını göstermiştir. Ayrıca, mutasyon verileriyle entegrasyon sonucunda, nöronal mesane kanserinde nöronal olmayanlara kıyasla önemli ölçüde daha yüksek onkojenik ekzon 3 ß-catenin mutasyonlarının olduğu belirlendi. İkinci olarak, deneysel teknikler kullanılarak mesane kanserindeki epigenetik deregülasyonunun araştırılması hedeflendi. Bu amaçla, mesane kanserinde en sık mutasyona uğrayan kromatin düzenleyici olan KDM6A genine odaklanıldı. KDM6A yokluğunda mesane kanserinin fenotipik ve epigenomik profilinin nasıl etkilendiğini araştırmak için kasa invaziv mesane kanseri karakterine sahip 5637 hücre hattında KDM6A geni knock-out edildi. Hücrelerin uzun süreli büyümesinde 5637 ve KDM6A-null 5637 canlılıkları arasında önemli bir değişiklik saptanmadı. Kromatin düzenleyici gen olan HDAC1 gibi kromatin organizasyon yolağında görev alan genlerin görece yüksek sinyallere sahip olduğu belirlendi. Bulgularımız, kromatin düzenleyici KDM6A yokluğunda baskılayıcı kromatin durumlarının artabileceğini göstermektedir, fakat gelecekte daha ayrıntılı bir şekilde araştırılması planlanmaktadır.

## 1. INTRODUCTION AND AIM

Bladder cancer is one of the most common types of cancer that is histopathologically heterogeneous and results around 200,000 deaths per year(1). Bladder cancer is most commonly caused by the urothelium (90%) and about 10% by squamous cell, small-cell or adenocarcinoma. Approximately 75% of patients have non-muscle-invasive bladder cancer, while the remaining 25% have muscle-invasive bladder cancer (2) Although NIMBC has a better prognosis, there is a chance that approximately 15% of NMIBC cases progress into MIBC (3).

There are recent studies to determine the mutation profile and molecular subclasses of bladder cancer (4). These studies have provided important information in for highly mutated genes that are likely to play a role in tumor formation in bladder cancer, and in categorizing bladder cancer into subclasses according to gene expression profiles. All these studies show that genes involved in chromatin regulation are highly mutated in bladder cancer. For this reason, bladder cancer is considered as a chromatin disease.

The aim of this thesis is to determine epigenetic regulatory profiles in bladder cancer using computational and experimental approaches. Firstly, the muscle-invasive bladder cancer ATAC-Seq data from Corces et al. (5), published in 2018, will be analyzed and this data will be integrated with various datasets to understand the molecular mechanism of muscle-invasive bladder cancer. For this purpose, R programming language (6) will be used. Secondly, the Lysine Demethylase 6A (KDM6A) gene, which is a chromatin regulator gene that is frequently mutated in bladder cancer, will be investigated. A muscle-invasive bladder cancer cell line “5637” will be used as a model for this research. For this, KDM6A gene will be knock-out using the CRISPR-Cas9 method, which is frequently used in the analysis of molecular mechanisms, and the changes on chromatin will be investigated by Chromatin Immunoprecipitation Sequencing (ChIP-Seq) method.

## 2. GENERAL INFORMATION

### 2.1. Epigenetic Mechanisms

It is known that genomic alterations on DNA especially on important genes initiates many diseases including cancer (7). Over the last decades, an unfamiliar mechanism emerged called epigenetics. Chromatin is a highly dynamic and organized structure that consist of DNA and relevant proteins called histones (8). Epigenetics is a term that describes the modifications on chromatin without the changes on DNA sequence. Epigenetic modifications are reversible on the contrary of genomic mutations. These modifications include DNA methylation, histone post-translational modifications and non-coding RNA based mechanisms (9). Epigenetic mechanisms also have a role in initiation and progress of several diseases including cancer (10).

#### *2.1.1 Histone Modifications and Chromatin Remodeling*

In the early days, researchers mostly focused on the effect of DNA methylation on disease formation. In the meantime, evidence raised pointing out epigenetic mechanisms other than DNA methylation that can be equally important in disease formation including cancer (11). Chromatin remodeling is one of the critical players of epigenetic regulation and regulated by post-translational histone modifications, interaction with transcription factors and other chromatin factors (12). Chromatin regulators can be divided into several groups based on their mechanism of action, mainly as readers, writers and remodelers (12).

Proper action of chromatin regulators is required for normal cellular processes and development. Chromatin regulators establish different configuration of epigenetic states at different sites of genomic regions. Inactive parts of the genome are as associated with repressive chromatin states while active parts are as associated with active chromatin states (Figure 1). H3 lysine 9 trimethylation (H3K9me3) is a classical heterochromatin mark while broad Polycomb repressed regions mostly have the repressive H3K27me3 mark. H3K27me3 state is controlled by EZH2 and KDM6A equilibrium. KDM6A is a demethylase which removes methyl

groups from H3K27me3 and EZH2 is a methyltransferase, component of Polycomb repressor complex 2 (PRC2), which catalyze addition of methyl groups. Active regions of the genome - especially enhancer and promoter regions – have mostly H3K4 methylation and H3K27 acetylation. H3K4 methylation is catalyzed by MLL family proteins. Proteins of this family are members of different COMPASS methyl transferase complexes and are important for both tumor formation and reprogramming (13). H3K27ac mark is controlled by histone acetyl transferases (HATs) and histone deacetylases (HDACs). This mark is mostly present on active enhancer regions of the genome (12).

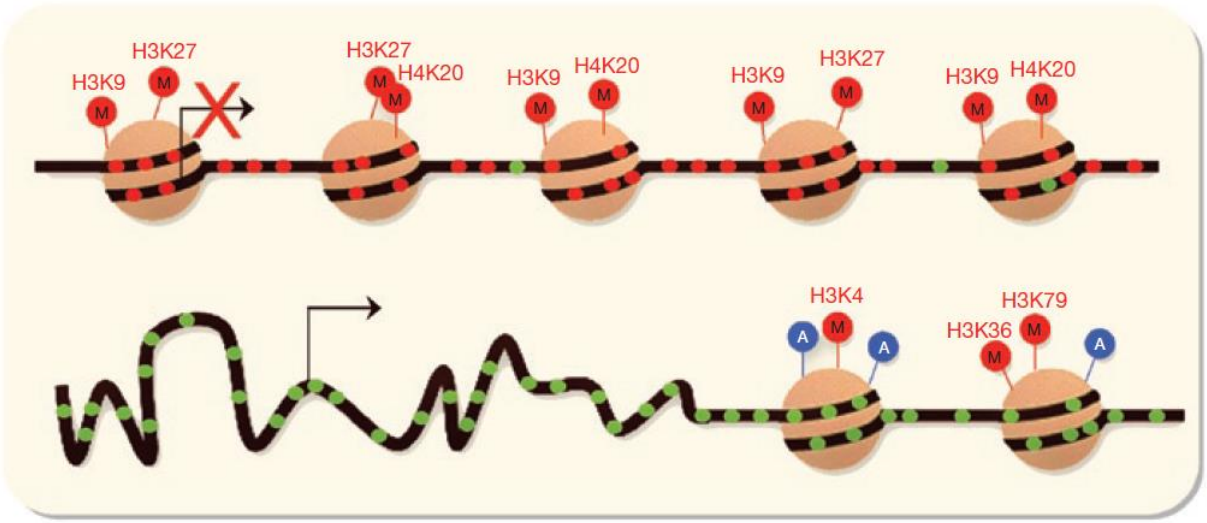


*Figure 1. Histone modifications in transcriptional regulation (Adapted from (14), LN: 5118370216027)*

### *2.1.2 Active chromatin regulatory elements*

Regulatory elements are specific regions in genome critical for gene regulation. Promoters and enhancers are the primary regulatory elements. They establish cell type identity by interacting with transcription factors and regulating

gene expression (15). Active regulatory elements are located at open regions of the genome and are accessible for protein binding (16).

ATAC-Seq is a widely used technique to determine active regulatory elements in the genome. This assay basically makes use of Tn5, which is a prokaryotic transposase enzyme and has specific point mutations that enhance its transposase activity at open chromatin regions. Use of this enzyme also enables insertion of adapters to the accessible regions of the chromatin, required for high-throughput sequencing of open chromatin regions (Figure 2). The most distinctive and advantageous feature that distinguishes this method from its alternatives (ChIP-seq, DNase-seq, MNase-seq) is the requirement of only 50,000 cells (17).

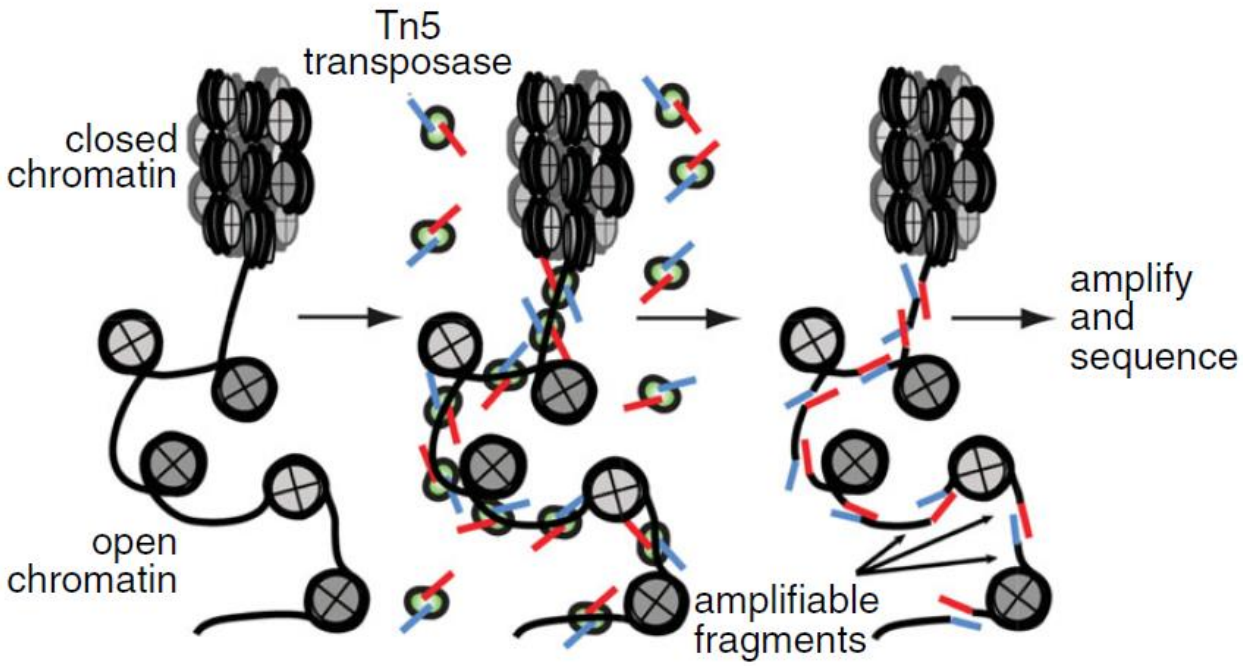


*Figure 2. ATAC-seq technique schematic (Adapted from (17), LN: 5118370648688)*

### *2.1.3 Lysine Demethylase 6A (KDM6A)*

KDM6A is known as a Histone H3 lysine 27 demethylase. But many studies have shown that it has functions apart from H3K27 demethylation activity. KDM6A interacts with H3K4 methyl transferases MLL3/4, H3K27 acetyltransferases and also with SWI/SNF chromatin remodeling complex. KDM6A has important roles in early development, tissue specific development and stem cell differentiation. It is known to be a tumor suppressor and frequently mutated in many cancer types, especially in bladder cancer. Bladder cancer has the most frequent KDM6A mutations with 29% (18). This ratio might be slightly vary between studies since mutation rates differ between muscle invasive and non-muscle invasive bladder cancer samples (19).

Proper and balanced function of KDM6A is necessary for normal cellular development (19). Loss of KDM6A disrupts the EZH2/KDM6A epigenetic switch which leads to EZH2 mediated transcriptional repression (Figure 3). There are several studies which support the tumor suppressive role of KDM6A. One study showed that wild-type expression of KDM6A caused deceleration of cell growth in KDM6A-absent esophageal squamous carcinoma cells (20). In a bladder cancer cell line, the loss of KDM6A increased the proliferation of the cells by 25% (19).

The absence of KDM6A reduces the expression of tumor suppressor genes such as CDKN1A and PERP. In a KDM6A null bladder cancer cell line reintroduction of WT or catalytically dead KDM6A slowed the colony formation and proliferation of the cells (21). This study also suggests that the tumor suppressor function of KDM6A is mostly independent from its catalytic -demethylase- domain.

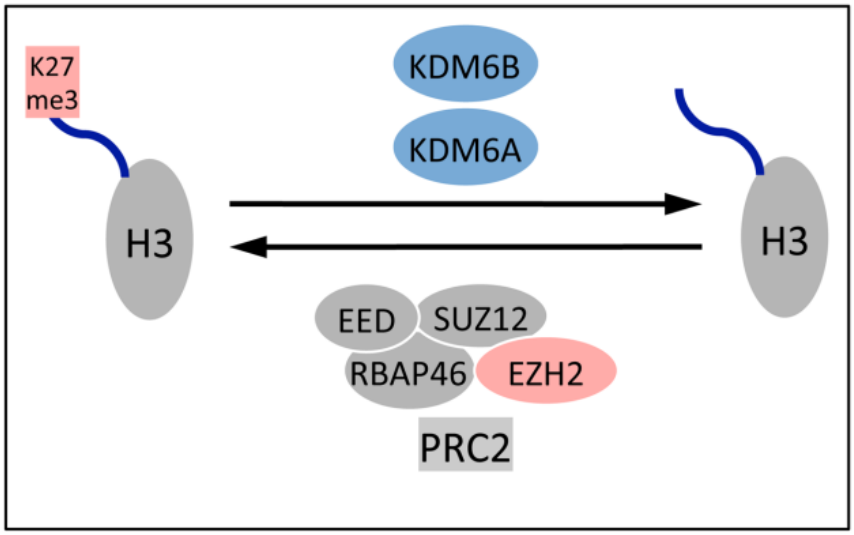


*Figure 3. Polycomb mediated gene silencing (Adapted from (22))*

### *2.1.4 H3K4me3 (Histone 3 Lysine 4 Trimethylation) Histone Mark and H3K4me3 breadth*

H3K4me3 is an active chromatin mark which is present mostly at promoter regions as narrow peaks (23). A study has showed that 80% of the genes that contain H3K4me3 mark at their promoter regions have active transcription in human embryonic stem cells (24). But it is also known that transcription can occur without the H3K4me3 mark at the promoter regions of the genes (25). Thus, the mechanism underlying the link between transcription and H3K4 methylation has not been fully understood yet.

Recent studies have also identified broad H3K4me3 peaks and showed that it has some important roles in regulation of transcription in various cell types (Figure 4) (26).

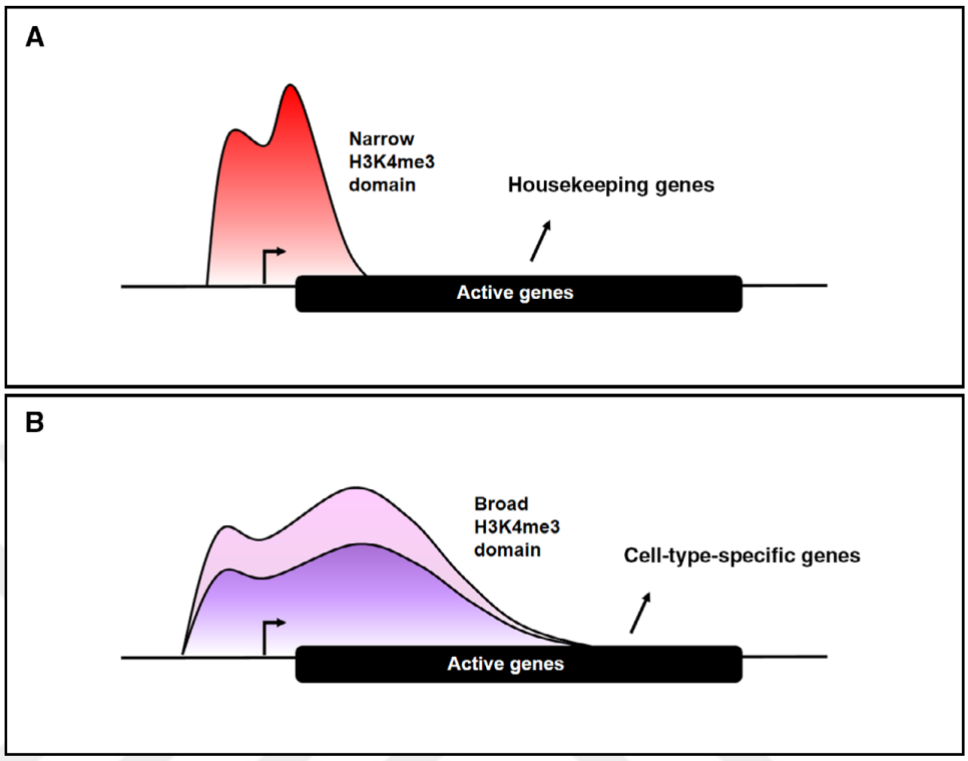


*Figure 4. Narrow and broad H3K4me3 domains (Adapted from (23))*

A study has shown broad H3K4me3 peaks (wider than 4 kb) downstream of tumor suppressor genes that have increased transcriptional activity in normal cells. Tumor suppressor genes had broader and more conserved H3K4me3 signature than housekeeping genes and oncogenes. In the same study, the authors also observed shortening of the broad H3K4me3 peaks at tumor suppressor genes in 20 different cancer cell lines. Besides, the reduced expressions of tumor suppressor genes have been identified in these cancer cell lines. Eventually, the association between shortening of the broad H3K4me3 signatures and repression of the tumor suppressor genes have emerged in cancer cells (27).

### *2.1.5 KDM6A and H3K4me3 interplay*

KDM6A functions together with H3K4 methyltransferases (28) and there are few studies that have discovered the relationship between KDM6A gene function and H3K4me3 mark. A previous study identified that the UTX null iNKT cells showed decreased H3K4me3 and increased H3K27me3 at the promoters of iNKT

cell signature genes occupied by KDM6A (29). In another study, the authors have showed that inhibition of H3K27 demethylases, KDM6A and KDM6B, induce apoptosis of the five human chordoma cell lines and also investigated the effects of dual inactivation of these genes via CRISPR/Cas9 on histone signatures. Absence of these genes in chordoma cell lines led to genome-wide elevated levels of repressive H3K27me3 marks and decreased levels of active H3K4me3, H3K9Ac and H3K27Ac signatures (30). A recent study also has shown the altered H3K4me3 levels as a consequence of KDM6A knock-down. It was identified that non-small cell lung cancer (NSCLC) patients with poor prognosis had high expression levels of KDM6A and in. when KDM6A was knock-down in NSCLC cell lines, proliferation of the cells has decreased. The knockdown also altered the signature of H3K4me3 but not H3K27me3, indicating the possible catalytically independent function of KDM6A (28).

## 2.2. Bladder Cancer

### *2.2.1 Bladder cancer as a disease*

Bladder cancer is one of the most frequent cancer worldwide with over 500,000 new cases and around 200,000 deaths in 2018 (1). Lifetime risk of bladder cancer is 1.1% in men and 0.27% in women (31). The primary risk factor for bladder cancer is tobacco smoking (32).

Most of the bladder cancers are called as urothelial bladder cancer as they mostly originate from urothelium. Bladder cancer is classified in two groups histopathologically; muscle invasive bladder cancer (MIBC) and non-muscle invasive bladder cancer (NIMBC). Around 25% of the bladder cancer patients suffer from MIBC while 75% are diagnosed with NIMBC (2). Although NIMBC has a better prognosis, there is a chance that approximately 15% of NMIBC cases progress into MIBC (3).

### *2.2.2 Current situation with the diagnosis and treatment of bladder cancer*

Bladder cancer is generally a disease of middle aged and elderly (33). In fact, age is one of the strongest risk factors for bladder cancer development. The highest incidence of bladder cancer occurs at 85 years old (33). Most common diagnostic factor for bladder cancer is visible hematuria. Endoscopic or transurethral resection of the tumor is diagnostic and potentially therapeutic (34). Current treatment options both for NMIBC and MIBC are rather unspecific, largely consisting of transurethral resection of bladder, Bacille Calmette-Guérin (BCG) application and chemotherapy for NMIBC and mainly neoadjuvant chemotherapy prior to radical cystectomy for the treatment of MIBC patients (34). Recently, MIBC patients receiving neoadjuvant systemic immunotherapy with pembrolizumab showed promise. 42% of MIBC patients downgraded to pT0 stage with this treatment (35).

### *2.2.3 Bladder cancer genomics and molecular subtypes*

Obtaining genomic, epigenomic and transcriptomic information has become easier over the last decades due to advances in next generation sequencing techniques. There have been several studies which aimed to identify the molecular subtypes of both muscle invasive and non-muscle invasive bladder cancer (Figure 5). These classifications were generally done according to tumor samples' transcriptome profiles. These studies also revealed the mutational landscape of bladder cancer.

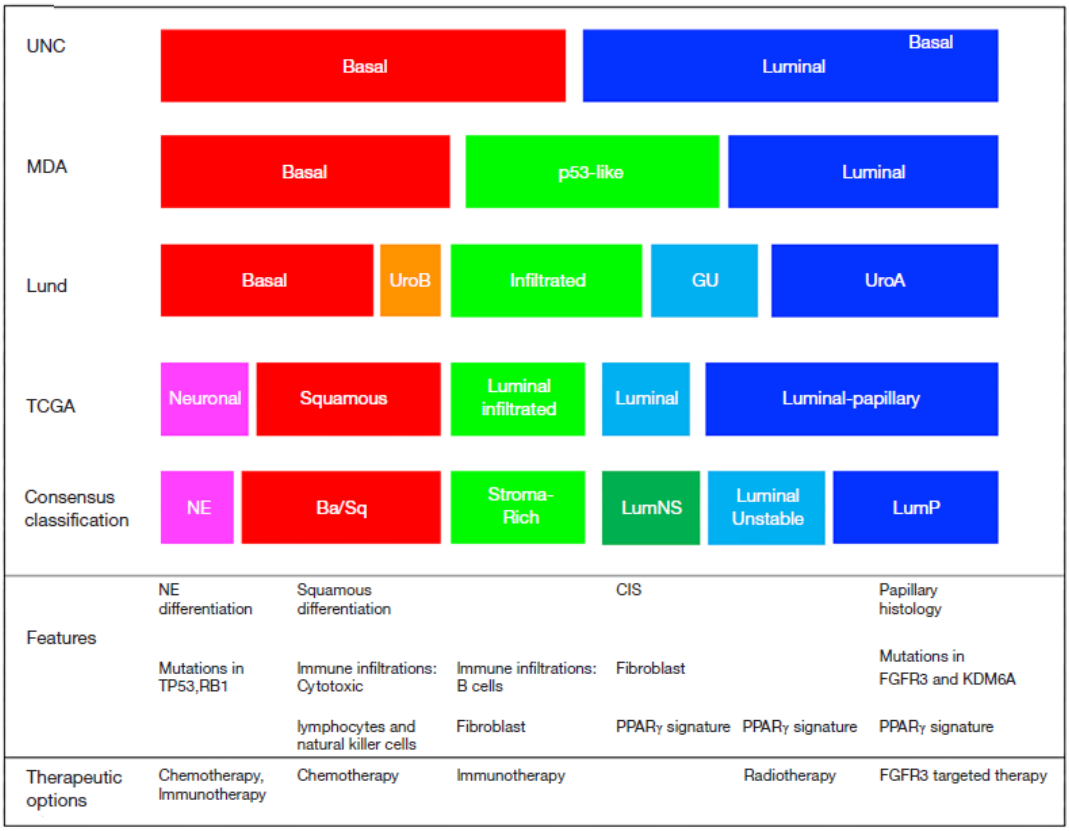


*Figure 5. Molecular subtype classifications of bladder cancer (Adapted from (36))*

In prior studies, unsupervised clustering analysis has been done to determine the gene expression profiles of bladder cancer and there was a clear distinction between NMIBC and MIBC samples (37). These each subtype was then divided into two major subgroups: luminal and basal (38, 39). In 2013, a study defined 5 molecular subtypes by combining MIBC and NMIBC datasets: urobasal A, genomically unstable, urobasal B, squamous cell carcinoma like, infiltrated (40). After that, in 2014 a study defined 4 MIBC TCGA subgroups (41). Subsequently, in the TCGA study performed in 2017 by Robertson et al. enhanced the prior 2014 classification and defined 5 MIBC subtypes according to the transcription profiles: neuronal, basal squamous, luminal, luminal infiltrated, luminal-papillary (4). Most recently Kamoun et al. used and integrated six published MIBC classifications to define a consensus classification for MIBC consisting of 6 subtypes: luminalpapillary: LumP, luminal-nonspecified: LumNS, luminal unstable: LumU,

stroma-rich, basal/squamous: Ba/Sq and neuroendocrine-like: NE-like (42). In this consensus classification study, identified classes were also associated with the clinical data, survival outcomes and therapeutic approaches. Recently, there was another study which defined the consensus classes of NMIBC (Class 1, 2a, 2b and 3) (43). Importantly, these two studies also generated a single-sample classifier tool named BLCAclassify for the classification of both MIBC and NMIBC (42, 43).

### *2.2.4 Epigenetic Mechanisms in Bladder Cancer*

Almost all the studies which characterize the mutational landscape of urothelial bladder cancer indicated the high mutation rate of genes involved in chromatin regulation (41, 44). Therefore, the deregulation of epigenetic mechanisms in bladder cancer is incontrovertible.

Mutation rates of genes that have roles in chromatin remodeling are very high in both NMIBC and MIBC bladder cancer. In bladder cancer, 89% of histone modifiers has been mutated (41). These mutations might have substantial impact on chromatin modifier function, ultimately resulting in chromatin deregulation and transcriptional mis regulation. Writer genes like EZH2 (Histone methyltransferase) and MLL (Lysine methyltransferase) family, eraser genes like KDM6A (UTX) are very important in the aspect of chromatin regulation. These genes are key factors for the balance between active and repressive chromatin states. Once this equilibrium is lost as a result of critical mutations in one of these gene groups epigenetic deregulation results in tumorigenesis (12). In bladder cancer the great majority of mutated epigenetic factors are involved in active chromatin organization (Figure 6) (4, 45).

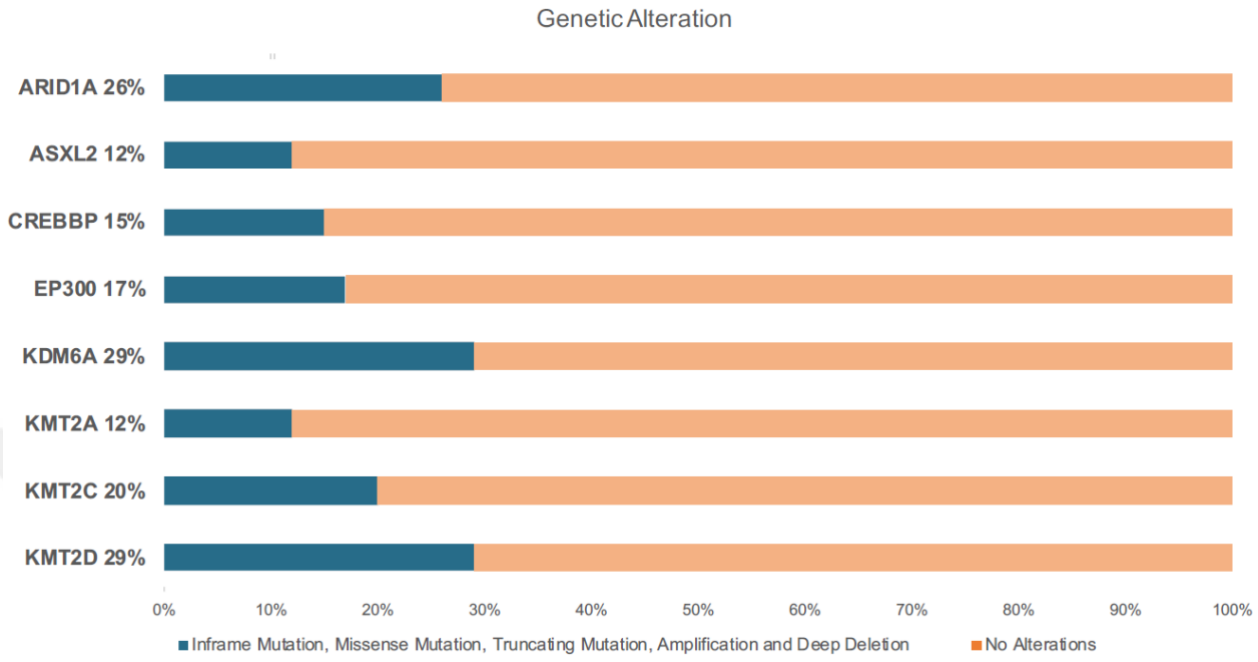


*Figure 6. Mutation frequencies of chromatin modifiers in bladder cancer (Adapted from (45), LN: 5124771508441)*

Deregulation of DNA methylation has also been also identified to be an important factor for bladder cancer. It is known that there are more than 50% changes in DNA methylation levels of analyzed bladder cancer cases (46). In fact, hypermethylation at promoter regions of many tumor suppressor genes has been identified (4, 12).

### 2.3. Role of Wnt/ß-catenin Pathway in Cancer

Wnt/ß-catenin pathway also known as canonical Wnt pathway has many critical roles in cell survival, development, differentiation, invasion, and migration (Figure 7) (47). Recent studies are pointing out the deregulation of canonical Wnt pathway, especially ß-catenin, in tumorigenesis and malignancies (48-50).

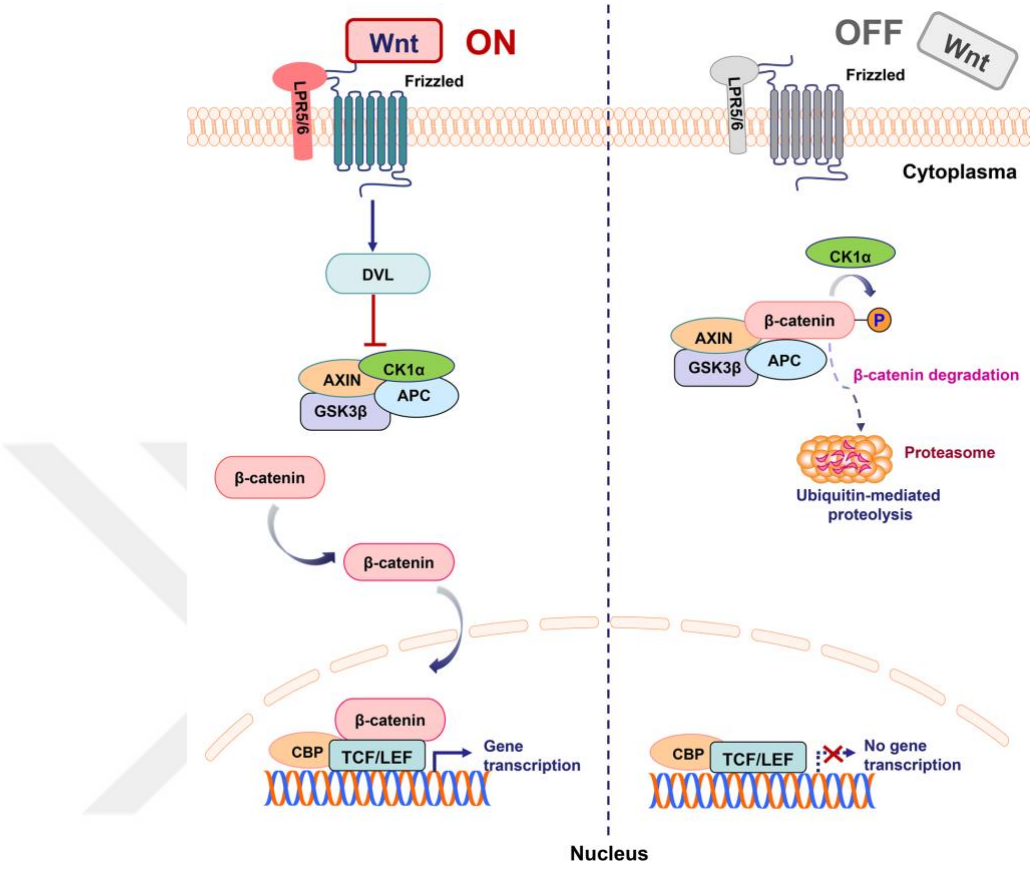


*Figure 7. Activation and inhibition of Wnt/ß-catenin pathway (Adapted from (47))*

Normally, localization and level of ß-catenin are controlled by ß-catenin destruction complex components; GSK3ß, Ck1a, Axin and APC, phosphorylating and ubiquitinating ß-catenin, resulting its degradation in the absence of canonical Wnt ligand. However, in the presence of Wnt ligand the ß-catenin destruction complex disassembles, and ß-catenin accumulates in the cytoplasm. Dephosphorylated ß-catenin migrates to nucleus and as a co-regulator interacts with TCF/LEF transcription factor. This leads to the activation of Wnt targets such as c-Myc and CDKN1A (47, 51).

Proper regulation of ß-catenin and TCF/LEF mediated transcription is important for proliferation, survival and stemness of the cells. ß-catenin over activity can be achieved through two main ways. One way is the mutations that inactivate the destruction complex components (*AXIN1*, *AXIN2*, *APC*) and mutations of ß-

catenin causing its overexpression/accumulation. The other way is the loss of negative feedback loop between Wnt receptor and RNF43, ZNRF43. Loss of Wnt receptor inhibitors (RNF43, ZNF43) leads to the accumulation of Wnt receptors and subsequently overactivation of Wnt pathway. Either way these events induce Wnt dependent tumor formation (52).

### *2.3.1 Role of Exon 3 ß-catenin Mutations in Cancer*

Many studies have showed that the mutations in ß-catenin gene are involved in tumor formation. High frequency of ß-catenin mutations is found in many cancer types (53). Although most of the ß-catenin mutations have an effect on oncogenesis, especially exon 3 mutations have been indicated as highly oncogenic (54). These exon 3 mutations, especially on S33, S37 and S45 positions prevent the phosphorylation and ubiquitination of ß-catenin and cause its nuclear accumulation (55, 56). Thus, ß-catenin activates the target genes which are advantageous for survival and proliferation of the cells.

## 3. MATERIALS AND METHODS

### 3.1. Research Type

This study is a both experimental and computational study.

### 3.2. Time and Place of the Study

This study was conducted at İzmir Biomedicine and Genome Center, between January 2019 and June 2021.

### 3.3. Research Materials

5637 human bladder cancer cell line purchased from DSMZ (German Collection of Microorganisms and Cell Cultures GmbH) was used in this study.

### *3.3.1 Laboratory Equipments and Supplies*

Laboratory equipments and supplies used in this study and their supplier companies are shown in Table 1 and 2, respectively.

*Table 1. Laboratory equipments used in this study and their supplier companies.*

| **Equipments** | **Company** |
|---|---|
| Micropipettes | 2 µl, 10 µl, 20 µl, 200 µl, 1000 µl Gilson |
| Microcentrifuge | Thermo Scientific Micro CL 17R 230 V. |
| PowerPac™ Basic Power Supply | Bio Rad |
| Mini Electrophoresis System | Thermo Scientific OWL B1A |
| Centrifuges | Eppendorf 5810 R |
| Human Cell Culture Incubator | memmert |
| Bacterial $CO_2$ Incubator | Heracell |
| Nanodrop | Thermo Scientific Nanodrop 2000 |
| Class II Biological Safety Cabinets | Thermo Scientific Safe 2020 |
| Benchtop Orbital Shaker | Thermo Scientific MaxQ 4000 |
| Sonicator | Covaris S220 |
| Water Tank | Nuve NB9 |
| Light Microscope | ZEISS Vert.A1 |
| Hemocytometer | ISOLAB |
| Ice Machine | HOSHIZAKI |
| Freezer (-20) | Bosch - GSN 51 AW |
| Cell Sorter | BD FACSAria III |
| Microplate Spectrophotometer | Thermo Scientific Multiskan GO |
| Freezer (-80) | New Brunswick |
| Western Blot System | BIO-RAD |
| Electronic pipettor | ISOLAB |

| | |
|---|---|
| Fume Hood | Kötterman 2-401-GAAAAY |
| Thermal Cycler | Simpleamp A24811 |
| Mini Vortex Mixer | Thermo Scientific ELED-88880018/ LPMixer |
| Tube Rotator | Thermo Scientific Eled 88881002 |
| Micro Centrifuge | Thermo Scientific TS-75004061 mySPIN |
| Lab Scale | Sartorious ENTRIS 822-1S Model |
| Volume Measuring Equipments | ISOLAB |
| Magnetic stirrer | Thermo Barnstead / BS-SP131320-33Q |
| pH meter | Hanna ELED Model |
| Erlens | ISOLAB |
| Cool Rack | Corning |
| Mr. Frosty Freezing Container | Thermo Fisher Scientific |
| Washing Bottles | ISOLAB |
| Borosilicate Glass Bottles | ISOLAB |
| Spray Bottles | ISOLAB |
| Spatula set | ISOLAB |
| DYNAL DynaMag Dynabeads DynaMag 2 Magnet | Thermo Fisher Scientific |
| Real-Time PCR System | Applied Biosystems 7500 Fast |
| Western Blot Membrane Imaging System | LI-COR ODYSSEY CLx |
| Digital Heating Shaking Drybath | Thermo Scientific #88880028 |
| Gel Documentation System | BIO-RAD Gel Doc XR+ |

*Table 2. Laboratory supplies used in this study and their supplier companies.*

| **Supplies** | **Company** |
|---|---|
| Cell culture dishes | Corning |
| Cryogenic tubes | Corning |
| Cell scrapers | ISOLAB |
| MicroAmp™ Fast Optical 96-Well Reaction Plate | Thermo Fisher Scientific 4346906 |
| Bacteria culture dishes | FIRATMED |
| Multiwell plates | Corning |
| Vacuum filtration system | Milipore |
| Syringe Filters | Set medikal |
| Cell Strainers | Sigma-Aldrich |
| Falcons (15 ml, 50 ml) | SPL |
| PCR tubes | Neptune |
| Examination Gloves | ISOLAB |
| Serological Pipettes | SPL |
| Eppendorf tubes (0.5 ml, 1.5 ml, 2 ml) | Thermo |
| Disposable pipette tips | Neptune |
| Nitrocellulose membrane | BIO-RAD |
| Color Prestained Protein Standard | NEB P7719S |
| Glass Pasteur Pipette | ISOLAB |
| DNA LoBind Tube (1.5 ml) | Eppendorf |

### *3.3.2 Commercial Kits*

Commercial kits used in this study and their supplier companies are shown in Table 3 below.

*Table 3. Commercial kits used in this study and their supplier companies.*

| **Kit** | **Company** |
|---|---|
| Pierce™ BCA Protein Assay Kit | ThermoFisher Scientific 23227 |
| FastStart Essential DNA Green Master | Roche 06402712001 |
| DNA Clean & Concentrator | Zymo Research D4034 |
| EZ-PCR Mycoplasma Detection Kit | Biological Industries 20-700-20 |
| Plasmid DNA Purification (Midi) | Macherey-Nagel 740412.10 |
| Plasmid DNA Purification (Mini) | Macherey-Nagel 740588.50 |
| PCR clean-up Gel extraction | Macherey-Nagel 740609.50 |
| Cell Proliferation Kit I (MTT) | Roche 12352200 |
| OneTaq ® Hot Start Quick-Load 2X Master Mix | New England Biolabs M0488S |
| Mix & Go E. coli Transformation Kit & Buffer Set | Zymo Research T3001 |
| Lipofectamine 3000 Reagent | ThermoFisher Scientific L3000001 |
| Quick-DNA™ Miniprep Plus Kit | Zymo Research D4068 |

### *3.3.3 Cell Culture*

Cell culture media and solutions used in this study are shown in Table 4 below.

Complete RPMI growth medium was prepared with %10 FBS and %1 Penicillin/Streptomycin.

*Table 4. Solutions used in cell culture studies.*

| **Solutions** | **Company** |
|---|---|
| Roswell Park Memorial Institute (RPMI) Medium | Gibco 11875101 |
| Fetal Bovine Serum (FBS) | Thermo Fisher Scientific 10500064 |

| | |
|---|---|
| Penicillin/Streptomycin | Thermo Fisher Scientific 15140122 |
| Gibco Trypan Blue | Thermo Fisher Scientific 15-250-061 |
| Freezing Medium | Thermo Fisher Scientific 12648010 |
| Phosphate-Buffered Saline (PBS) | Thermo Fisher Scientific 70011036 |
| TrypLE | Thermo Fisher Scientific 12604013 |
| Opti-MEM | Thermo Fisher Scientific 31985062 |

### *3.3.4 General Chemicals*

General chemicals used in this study are shown in Table 5 below.

*Table 5. General chemicals used in this study.*

| **Chemical** | **Company** |
|---|---|
| EDTA | Sigma-Aldrich SRE0033-1L |
| Ethanol | Merck 100983.2511 |
| Methanol | Sigma-Aldrich 32213-2.5L |
| NaCl | Sigma-Aldrich S5886-500G |
| Glycerol | Sigma-Aldrich G9012-100ML |
| Phosphate Buffer Saline (10X) | Thermo Fisher 70011036 |
| TritonX-100 | Sigma-Aldrich T8787-100ML |
| Na deoxycholate | Sigma-Aldrich D6750-10G |
| SDS | Invitrogen 24730020 |
| Tris | Sigma-Aldrich 648314-100ML |
| EGTA | Sigma-Aldrich 324626-25GM |
| Protease inhibitor coctail | Roche 11836153001 |
| Glycine | Sigma-Aldrich G7403-100G |
| HCl | Sigma-Aldrich 320331-500ML |
| Tween-20 | Sigma-Aldrich P1379-100ML |

| | |
|---|---|
| Ponceau | Sigma-Aldrich P3504-10G |
| Acetic Acid | Sigma-Aldrich 27225-2.5L-R |
| Formaldehyde | Sigma-Aldrich 252549-1L |
| Tris Acetate-EDTA (TAE) Buffer (10X) | Sigma-Aldrich T9650-1L |
| Agarose | Sigma-Aldrich A9539-100G |
| Isopropanol | Sigma-Aldrich 563935-1L |
| B-mercaptoethanol | Sigma-Aldrich 444203-250ML |
| Bromophenol blue | Sigma-Aldrich B0126-25G |
| TEMED | Sigma-Aldrich 1107320100 |
| 10% APS | Biofroxx 1610GR100 |
| Protogel | National Diagnostics EC-891 |
| Skim milk powder | Sigma-Aldrich 70166-500G |
| $NaHCO_3$ | Sigma-Aldrich S5761-500G |
| LiCl | Sigma-Aldrich L9650-100G |
| TERGITOL™ NP-40 (70%) | Sigma-Aldrich NP40S-100ML |

### *3.3.5 Bacteria*

Stbl3 and 10-beta *E.coli* strains are kindly provided by Doc. Dr. Şerif Şentürk from İzmir Biomedicine and Genome Center.

Bacteria were spreaded on Bacteriological Agar plates which contain 1X Ampicillin antibiotic and grown in LB medium that contains 1X Ampicillin antibiotic. Components of bacteriological agar plates are shown in Table 6 and Table 7, respectively.

*Table 6. Components of Bacteriological Agar Plates (for 1L).*

| **Component** | **Amount** | **Company** |
|---|---|---|

| | | |
|---|---|---|
| Bacteriological Agar | 35 g | Caisson Labs LBP04-500GM |
| Ampicillin (1000X) | 1 ml | BioFroxx |
| $ddH_2O$ | 1 L | - |

*Table 7. Components of LB Broth Medium (for 1L).*

| Component | Amount | Company |
|---|---|---|
| Tryptone | 10 g | Biolife |
| Yeast Extract | 5 g | Sigma-Aldrich R8508-1ML |
| NaCl | 10 g | Sigma-Aldrich S5886 |
| $ddH_2O$ | 950 ml | - |

### *3.3.6 Antibodies*

Antibodies used in this study shown in Table 8 below.

*Table 8. Antibodies used in this study and their supplier companies.*

| Antibody | Company | Cat. No. |
|---|---|---|
| UTX (D3Q1I) Rabbit mAb | Cell Signaling Technology | #33510 |
| Histone H3K4me3 antibody (pAb) | Active Motif | #39.159 |
| β-Actin (8H10D10) Mouse mAb | Cell Signaling Technology | #3700 |
| Anti-rabbit IgG (H+L) (DyLight™ 800 4X PEG Conjugate) | Cell Signaling Technology | #5151 |
| IRDye® 680LT Goat anti-Mouse IgG Secondary Antibody | Li-COR | 926-68020 |

### *3.3.7 Western Blot Buffers*

Ingredients of buffers used in Western Blot experiment are shown in Table 9, Table 10, Table 11, Table 12, Table 13, Table 14, and Table 15.

*Table 9. Components of RIPA Buffer (1X / 50 ml).*

| **Component** | **Amount** |
|---|---|
| Triton X-100 (10%) | 5 ml |
| Na deoxycholate (10%) | 2.25 ml |
| SDS (20%) | 250 µl |
| Tris-Cl pH 7,4 (1M) | 2.5 ml |
| NaCl (5M) | 1.5 ml |
| EDTA pH 8 (0,5M) | 100 µl |
| EGTA (0,1M) | 500 µl |
| Protease Inhibitor Cocktail (for 1 ml) | 40 µl |

*Table 10. Components of Running Buffer (10X / 1L) pH~8,3*

| **Component** | **Amount** |
|---|---|
| 250 mM Tris base | 30.2 g |
| 1,9 M Glycine | 142 g |
| 1% SDS | |

*Table 11. Components of Transfer Buffer (10X / 1L) pH~8,3*

| **Component** | **Amount** |
|---|---|
| 250 mM Tris base | 3.02 g |
| 1,9 M Glycine | 14.2 g |
| 20% methanol (add before use) | 200 ml |

*Table 12. Components of TBS (10X / 1L) pH~7,6*

| Component | Amount |
|---|---|
| Trizma HCl | 24.23 g |
| NaCl | 80.06 g |

*Table 13. Components of TBST (1X / 1L)*

| Component | Amount |
|---|---|
| TBS (10X) | 100 ml |
| $dH_2O$ | 900 ml |
| Tween-20 | 1 ml |

*Table 14. Components of Ponceau Dye*

| Component | Amount |
|---|---|
| Acetic Acid | 0.5 ml |
| Ponceau | 0.25 ml |
| $dH_2O$ | 50 ml |

*Table 15. Components of Laemmli Buffer*

| Component | Amount |
|---|---|
| 0.5 M Tris-HCl (pH=6.8) | 20 ml |
| Glycerol | 20 g |
| SDS | 4 g |
| Bromophenol Blue | 0.05 g |
| 1M DTT | 2 ml |
| $dH_2O$ | 13 ml |

### *3.3.8 Plasmid Vector Cloning*

Plasmids, enzymes gRNAs and primers used in this study are shown in tables below. Restriction enzymes NheI and XhoI used for plasmid cloning are kindly provided by Doc. Dr. Şerif Şentürk from İzmir Biomedicine and Genome Center.

*Table 16. Plasmids used for cloning.*

| **Plasmid** | **Company** | **Cat. No.** |
|---|---|---|
| pSpCas9(BB)-2A-GFP (PX458) | addgene | #48138 |
| pCMV-HA-UTX | addgene | #24168 |
| pUltra-hot | addgene | #24130 |

*Table 17. Restriction enzymes used for cloning plasmids.*

| **Enzyme** | **Company** | **Cat. No.** |
|---|---|---|
| BbsI-HF | New England Biolabs | #R0539 |
| FastAP Thermosensitive Alkaline Phosphatase | ThermoFisher Scientific | #EF0651 |
| T4 Polynucleotide Kinase | New England Biolabs | #M0201S |
| T4 DNA Ligase | New England Biolabs | #M0202 |
| NotI-HF | New England Biolabs | #R3189S |
| KpnI-HF | New England Biolabs | #R3142S |
| SalI-HF | New England Biolabs | #R3138S |

*Table 18. gRNAs used in this study and their sequences.*

| gRNA Name | Forward Primer | Reverse Primer |
|---|---|---|
| KDM6A g312 | caccgTTGGATAATCTTCCAATAAG | aaacCTTATTGGAAGATTATCCAAc |
| KDM6A g43 | caccgGCCGCCGCTTTCGGTGATG | aaacCATCACCGAAAGCGGCGGCc |
| KDM6A g47 | caccgTTCCTCATCACCGAAAGCGG | aaacCCGCTTTCGGTGATGAGGAAc |
| REN g208 | caccgGTAGCGCGGTGTATTATACC | aaacGGTATAATACACCGCGCTACc |

*Table 19. Primers for validation of KDM6A knock-out via Sanger Sequencing.*

| Primer Name | Forward Primer | Reverse Primer |
|---|---|---|
| KDM6A g43, g47 | GGCGATAAAGTTGGTGTGCT | CTCTCCTCGGCTGTCAGG |
| KDM6A g312 | TAGGCTGTTCGCTGCTATGA | TTGCTCATGCACTTACAATTTC |

*Table 20. Primers for KDM6A Q555 point mutation.*

| Primer Name | Primer Sequence |
|---|---|
| Q555_F_1 Primer (Forward) | TCGACTGGATCCGGTACCTCCATGAAATCCTGCGGA |
| Q555_S1_R Primer (Reverse) | GCGGCCGCGAATTCGCCCTTCTAAGAGACGCTAGGCACTCT |

| | |
|---|---|
| KDM6A Q555 Mutation (Forward) | GTACCTCCATGAAATCCTGCGG |
| KDM6A Q555 Mutation (Reverse) | TGAGGCTAAGAGACGCTAGGC |

### *3.3.9 Chromatin Immunoprecipitation (ChIP)*

Ingredients of buffers used in ChIP experiments are shown in tables below. Primers for ChIP qPCR are also shown.

*Table 21. Components of Elution Buffer*

| **Component** | **Amount** |
|---|---|
| 10% SDS | 50 µl |
| 1M NaHCO3 | 50 µl |
| $dH_2O$ | 400 µl |

*Table 22. Components of DOC Buffer*

| **Component** | **Amount** |
|---|---|
| 1M Tris pH 8 | 20 µl |
| 1M LiCl | 0.5 ml |
| NP-40 | 10 µl |
| DOC (%10) | 0.1 ml |
| 0.5M EDTA | 4 µl |
| $dH_2O$ | 1366 µl |

*Table 23. Components of ParoFix*

| Component | Amount |
|---|---|
| 0.1M Hepes (pH 8.0) | 50 µl |
| 0.5M EDTA | 200 µl |
| 0.1M EGTA | 500 µl |
| 5M NaCl | 2 ml |
| 11% formaldehyde (add fresh before use) | |

*Table 24. Components of Paro Rinse 1*

| Component | Amount |
|---|---|
| 1M Tris (pH 8.0) | 5 ml |
| 0.5M EDTA | 10 ml |
| 0.5M EGTA | 0.5 ml |
| Triton X-100 | 1.25 ml |
| $dH_2O$ | 483 ml |

*Table 25. Components of Paro Rinse 2*

| Component | Amount |
|---|---|
| 1M Tris (pH 8.0) | 5 ml |
| 0.5M EDTA | 1 ml |
| 0.5M EGTA | 0.5 ml |
| NaCl | 20 ml |
| $dH_2O$ | 473 ml |

*Table 26. Components of Lysis Buffer*

| **Component** | **Amount** |
|---|---|
| 1M HEPES/KOH pH 7.5 | 25 ml |
| 5M NaCl | 50 ml |
| 0.5M EDTA | 1 ml |
| %100 Triton X-100 | 5 ml |
| %10 DOC | 5 ml |
| %20 SDS | 2.5 ml |
| $dH_2O$ | 411.5 ml |
| Add fresh: protease inhibitors | %4 |

*Table 27. Primers for ChIP qPCR.*

| **Gene** | **Forward Primer** | **Reverse Primer** |
|---|---|---|
| EIF4B | CAGTAATGGTAGACTCTGGCTTGA | CGGTGATTCACGTCTACGAA |
| RAB10 | AAGCGCTGTGCAGAGAAAC | CCGGGACACCCTTACAGAG |
| MCL1 | AATGAACCCCCTTACCTTGG | AAGCCAATGGGCAGGTCT |
| PRAC1 | TGGTCTGGAACTCCTGTGCT | AACATCTACTGGGCGAGACC |
| GABRA2 | TTTTCTTCACTCCCCTTAACAAA | GACTTGGTCTTGGGCAACC |
| DDIT4 | CCTTTGGGACCGCTTCTC | ATCTGGGGTGGGAGTTCG |
| TFAP2A | TATGGACATCGCGGCTCT | ATTTGCCTAAGCGATTCCAG |
| ATRAID | GCTACCCGAGGTACAGAAGC | AGCGTCAGGGACGAAATCAG |

### *3.3.10 Cell Sorting*

Ingredients of FACS Buffer used for cell sorting are shown in Table 28 below.

*Table 28. Ingredients of FACS Buffer.*

| Component | Amount |
|---|---|
| 1X PBS | 250 ml |
| %1 BSA | 2.5 g |
| %0.25 Na-Azide | 0.05 g |
| 1nM EDTA | 1 ml |

## 3.4. Variables of the Study

KDM6A expression levels of the 5637 cell line are independent variables of this study. Cell viability rates and chromatin states are dependent variables of this study.

## 3.5. Methods for Data Collection

### *3.5.1 Experimental Methods*

#### *3.5.1.1. Cell Culture*

##### *3.5.1.1.1. Thawing Frozen Cells*

Cryovial containing the frozen cells in Freezing Medium was removed from liquid nitrogen storage and immediately placed into 37°C water bath. Cells were thawed quickly in 37°C water bath until there is just a small bit of ice left in the cryovial. Then cells were transferred to 15 ml centrifuge tubes under the laminar flow hood. After that cell suspension was centrifuged at 1500 rpm for 4.5 minutes and the supernatant was removed carefully. Finally, cell pellet was gently re-suspended in pre-warmed complete RPMI growth medium and transferred into appropriate culture dish.

#### *3.5.1.1.2. Subculturing Adherent Cells*

First growth medium was removed and discarded from the culture dish. Cells were rinsed with 1X PBS carefully. Then appropriate amount of TrypLE was added directly onto cells dropwise until it covers the cell layer (1 ml TrypLE onto confluent 5637 on 10 cm human cell culture dish). After that, the culture dish was incubated at incubator for 5 minutes. After the detachment of the cells were observed under light microscope, pre-warmed complete growth medium was added on cells. Medium was dispersed by pipetting over the cell layer surface several times. Cells were transferred to a 15 ml centrifuge tube and centrifuged at 1500 rpm for 4.5 minutes. After that supernatant was removed carefully and cell pellet was resuspended with pre-warmed complete growth medium. Cells were counted and seeded to new cell culture dishes in appropriate amount.

#### *3.5.1.1.3. Freezing Cells*

Cells were detached from the cell culture dishes following the subculturing procedure. The total number of cells were determined, and cell suspension was centrifuged. After that, cells were resuspended with appropriate amount of ice-cold Freezing Medium ($1x10^6$/ml). Aliquots were transferred to cryovials and stored at -80°C in Mr. Frosty overnight. Then cryovials moved to and stored at -196°C in liquid nitrogen tanks.

### *3.5.1.2. KDM6A Knock-out with CRISPR-Cas9*

#### *3.5.1.2.1. Generating Competent Bacteria Strains*

To make Stbl3 and 10-beta competent *E.coli* strains, %25 glycerol bacteria stocks were used. The bacterial strain in 25% glycerol was removed from -80°C and thawed on ice. 5 ml LB medium was added to the 15 ml falcon by the fire. A scratch from the bacteria glycerol stock was taken with a micropipette tip and put in LB containing falcon. After that, bacteria containing falcon was put on bacteria orbital shaker at 225 rpm 37°C

overnight (16-18h). Next day, falcon was stored at +4°C until further application. After several hours, 50 ml Zymo Mix & Go Kit's Broth Medium and 500 µl of the grown bacteria strain was mixed in 250 ml flask. The flask was shaken at 250 rpm at 18°C overnight. In the following morning competent bacteria was obtained via applying Mix & Go E. coli Transformation Kit & Buffer Set protocol on ice. Isolated bacteria were aliquoted in 1.5 ml Eppendorf tubes 100 µl each and stored at -80°C.

#### *3.5.1.2.2. Target Guide Sequence Cloning*

To clone guide RNA sequences into PX458 plasmid vector three main steps were followed.

##### *3.5.1.2.2.1. Digestion and Dephosphorylation*

BbsI restriction enzyme was used for digestion and Fast AP (Alkalyne Phosohatase) was used for dephosphorylation. In a PCR tube, 5 µg PX458 plasmid DNA, 3 µl BbsI, 3 µl Fast AP, 6 µl 10x FastDigest Buffer were added and dd$H_2O$ was added up to 60 µl. Mix was incubated for 1 hour at 37°C. After the incubation 12 µl DNA loading dye was added to the mix and all mix was loaded to the %1 Agarose gel. Digested plasmid mix was run at 100V for 45 minutes. Agarose gel was visualized under UV light and the band at the expected plasmid location (~9000bp) was separated. Digested PX458 plasmid DNA was isolated using MN NucleoSpin Gel and PCR Clean-up Kit. DNA concentration was measured using Nanodrop 2000.

##### *3.5.1.2.2.2. Phosphorylation and Annealing of Oligos*

In PCR tubes, 1 µl of each pair of gRNA oligos (g43, g47, g312, REN g208) from 100 µM stocks, 1 µl 10X T4 Ligation Buffer, 0.5 µl T4 PNK and 6.5 µl dd$H_2O$ were added. Thermal Cycler parameters were set as follows; 30 minutes at 37°C, 5 minutes at 95°C and ramp down to

25°C (5°C/min). After that, oligo duplexes were diluted at 1/20 dilution with sterile water.

#### *3.5.1.2.2.3. Ligation*

In a PCR tube, 50 ng BbsI digested plasmid, 2 µl diluted oligo duplex, 1 µl T4 Ligation Buffer, 0.5 µl T4 Ligase and dd$H_2O$ up to 10 µl were added (for each reaction). Two negative controls were used: without oligo duplex and without T4 Ligase. Mixes were incubated at RT for 2 hours.

### *3.5.1.2.3. Transformation into Bacteria and Colony PCR*

Stbl3 bacteria strain was used for transformation of gRNA containing PX458 plasmid. First, one aliquot of competent Stbl3 for each sample was taken from -80°C and placed on ice until thawed. Previously ligated plasmids were added to melted Stbl3 containing eppendorfs by the fire. For positive control 100 ng uncut plasmid was used. Plasmid containing Stbl3 eppendorfs were incubated on ice for 30 minutes. After that, they were incubated at 42°C in water bath for 1 minutes then immediately put on ice for 5 minutes. 750 µl LB medium was added to the samples by the fire and incubated at 37°C for 45 minutes at 225 rpm on bacteria shaker. At the end of the incubation, samples were centrifuged with pulse for 10 seconds. Then, supernatant was discarded by the fire and pellet was resuspended with remaining LB. Transformed bacteria were then seeded at room temperature Ampicillin containing LB Agar plates by the fire. Plates were incubated overnight at 37°C in bacteria incubator.

In the following morning colony formation of the plates were observed. Only few numbers of colonies were observed in plates that have negative controls. Positive uncut control plate had too many colonies as expected. gRNA containing plates had expected number of colonies. Three colonies were picked from each gRNA plates with a pipette tip and dipped into PCR

tubes containing OneTaq ® Hot Start Quick-Load ® 2X Master Mix prepared for each gRNA with U6 forward primer and reverse gRNA primers. Remaining bacteria from the picked colonies were put into 1 ml LB medium and 1 µl Ampicillin containing eppendorfs with pipette tips. After that, remaining colony containing eppendorfs were incubated at 4°C until the colony PCR results came out. Samples were run on %2 Agarose gel at 90V for 40 minutes. All gRNA containing samples were had the band at the expected size. One colony was picked from each gRNA containing samples and grown in 15 µl Ampicillin containing 15 ml LB medium at 37°C 225 rpm on bacteria shaker overnight. gRNA containing plasmid DNAs were isolated with MN Mini Plasmid DNA Purification Kit. Necessary amount of the gRNA containing PX458 plasmids were sent to eurofins firm for Sanger Sequencing to validate the cloning.

#### *3.5.1.2.4. Transfection and Cell Sorting*

5637 bladder cancer cell line was used for transfection of KDM6A gRNA containing PX458 Cas9 plasmid. 5637 cell line was taken to the cell culture in complete RPMI media. Cells were passage into 5 different 60 cm cell culture plates to reach %70 confluency the day after for transfection. One of the plates was used as control for cell sorting. Remaining 4 cell plates were used for transfection. For each transfection, 250 µl Opti-MEM and 20 µl Lipofectamine reagent were mixed in a tube, 250 µl Opti-MEM 10 µl P3000 reagent and 5 ug plasmid DNA were mixed in another tube. Then the tubes were mixed together and incubated for 10 minutes at RT. After that, the transfection mixes were added to the relevant plates dropwise clockwise and plates gently swirled opposite of clockwise for droplets to disperse. Plates were incubated in human cell incubator. After 24 hours, GFP signal was observed in cells. 48 hours post transfection cells were prepared for cell sorting. First, all the media was collected and centrifuged, and supernatant was filtered to prepare condition media. 5 ml complete RPMI containing %2

Pen/Strep was added to the condition media. 100 µl of condition media was added to the each well of 96-well plate for each sample. Cells were rinsed with 1X PBS and collected using TrypLE. Then the collected cells were centrifuged, and the supernatant was discarded. Pellet was resuspended with 1 ml ice cold FACS Buffer. After that, cells were taken to the BD FACSAria III for sorting. The top %4 GFP positive cells were sorted as single cells on each well of condition media containing 96-well plates. Remaining GFP positive cells were sorted as bulk for latter protein isolation. Cells were left to grow at human cell incubator. After the single cells were grown, genomic DNA was isolated using Quick-DNATM Miniprep Plus Kit and gRNA target sequences were amplified using the primers from Table 19 for Sanger Sequencing.

#### *3.5.1.3. Protein Isolation and BCA Assay*

To isolate protein from 10 cm cell plates, plates were removed from the incubator and taken on ice. Growth media was vacuumed then cells were rinsed with 2 ml 1X ice cold PBS two times. 200 µl protease inhibitor cocktail containing 1X RIPA lysis buffer was added on cells. Then cells were scraped using cell scraper. Cells were collected in 1.5 ml eppendorfs. After that, cells were vortexed every 10 minutes for three times and in the meantime incubated on ice. Lysed cells were centrifuged at max speed at +4°C for 20 minutes. Protein containing supernatant was collected to another Eppendorf and pellet was discarded. Proteins were stored at -80°C until further use.

BCA Assay was performed to determine the protein concentrations. Pierce™ BCA Protein Assay Kit's protocol was followed. Protein standards was serially diluted six times with PIC containing RIPA buffer. All samples were triplicated included standards. 2 µl protein was added to the each well on 50 µl reagent mix in 96-well plate. Then plate was folded with aluminum folio for protect against light and incubated at 37°C for 30 minutes. Lastly, plate was

read with Multiskan GO microplate spectrophotometer and protein concentrations were determined.

#### *3.5.1.4. Western Blot*

For 1.5 mm glasses 10 ml %8 Separating gel was prepared for KDM6A Western Blot. For 10 ml %8 separating gel; 2.7 ml Protogel, 1.25 ml Main gel buffer, 5.05 ml dd$H_2O$, 50 µl %10 APS and 10 µl TEMED were mixed in a 15 ml tube and immediately loaded between the 1.5 ml glasses. Then, 1 ml %60 isopropanol was added to the top of separating gel to flatten the gel line and prevent bubbles. Gel was incubated for 15-20 minutes. After that, isopropanol was discarded, and gel was washed gently with water. For 4 ml stacking gel; 0.5 ml Protogel, 1 ml Protogel stacking buffer, 2.5 ml dd$H_2O$, 25 µl %10 APS and 5 µl TEMED were mixed in a 15 ml tube and loaded on frozen separating gel. Comb was set above stacking gel. Gel was incubated for 15-20 minutes. After the gel was frozen, comb was discarded gently, and wells were washed with water to get rid of the bubbles.

Glasses with gel were fixed to the PAGE device into the tank. Running Buffer was added up to the indicated point according to gel number. Protein samples prepared in advance and marker were loaded to the wells. Voltage was set to 90 V run for 30 minutes and then raised to 120 V run for ~1.5 hours.

For transfer step, gel containing glasses were opened in pure water. Stacking gel part was discarded to waste. 2 sponges and filter papers were wet in 1X transfer buffer. Transfer sandwich was prepared as follows, black side of the cassette, sponge, filter paper, gel, nitrocellulose membrane, filter paper, sponge, white side of the cassette. Sandwich was placed inside the tank and tank was put into a big washbowl filled with ice. PAGE device was set to 300mA and run for 1.5 hours.

After the transfer, membrane was blocked with %5 milk powder for 1 hour on shaker at 20 rpm. Then milk powder was discarded. KDM6A and ß-actin

antibody was diluted in %1 TBST 1:1000 and poured on the membrane and incubated overnight on shaker at 4°C 20 rpm. In the following morning, antibodies were collected, and membrane was washed with TBST on shaker at 50 rpm for 10 minutes three times. Secondary antibodies were diluted according to their datasheets and added to the membrane and shaken at 20 rpm for 1 hour RT. Membrane was washed again with TBST as before and then imaged with Li-COR device.

#### *3.5.1.5. Cell Viability Assays*

##### *3.5.1.5.1. MTT Assay*

To perform MTT assay, 2k cells for each well of 96-well plate both for 5637 and 5637 KDM6A knock-out cells were plated as triplicates and left to grow. Complete RPMI media was used as blank control. After 4 day, 10 µl MTT was added to all wells and incubated 4 hours at incubator. After 4 hours 100 µl solubilization buffer was added to the wells and incubated overnight. After incubation, 96-well plate wells were measured at 570nm wavelength with Microplate Spectrophotometer.

##### *3.5.1.5.2. Colony Formation Assay*

For colony formation assay, 500 cells were plated for both 5637 and 5637 KDM6A knock-out cells as triplicates to 6-well plate and incubated for 12 days at incubator. Mediums were changed every other day. After 12 days, cells were fixed with %3.7 formaldehyde for 20 minutes at RT. Then crystal violet solution (%10 ethanol, %0.1 crystal violet) was added on the cells and incubated for 40 minutes at RT. Cells were washed under stream of water. Plate was incubated overnight upside down to discard all water. Finally, plate was scanned with Li-COR device and then images were analyzed with ImageJ program.

#### *3.5.1.5.3. Cell Counting Assay*

For cell counting assay, 5637 and 5637 KDM6A knock-out cells were counted for 6 days. 5k cells were plated at each well of 24-well plate for both cell lines in duplicates. 2 wells of each cell line were counted with Hemocytometer under light microscope every day for 6 days.

### *3.5.1.6. Chromatin Immunoprecipitation (ChIP)*

H3K4me3 ChIP was performed in 5637 and 5637 KDM6A knock-out cells. Three %80 confluent 10 cm cell line plates were used for one ChIP experiment. Basically, the protocol from Weber et al. was followed with slight modifications (57).

10X formaldehyde solution was prepared with 1.46 ml Paro Fix and 0.54 ml formaldehyde. 1 ml 10X formaldehyde was added to a 10 cm cell plate and incubated 10 minutes at RT shaking. Crosslinking was stopped with 550 µl 2.5M Glycine for 10 minutes at 4°C. Cells were rinsed twice with 8 ml ice cold PBS on ice. Then 1 ml PBS was added, cells were scraped and collected in 15 ml tubes. After that, collected cells were centrifuged for 5 minutes at 600g at 4°C. Supernatant was discarded and cells were resuspended with PIC containing 12 ml Paro Rinse 1 and incubated on ice for 5 minutes. Then, supernatant was discarded, and pellet was resuspended with PIC containing 12 ml Paro Rinse 2. Cells were incubated on ice for 5 minutes. Cells were centrifuged again for 5 minutes at 600g 4°C. Lastly, supernatant was discarded, and pellet was resuspended with PIC containing 1 ml Lysis buffer. Cells were incubated on ice at least 10 minutes. 50 µl of the chromatin was taken as unsheared chromatin and kept on ice. Rest of the chromatin was sonicated for 7 cycles using Covaris sonicator. 50 µl of sonicated chromatin was taken as input chromatin. Then it was centrifuged at 14000 g for 10 minutes at 4°C and supernatant was taken. Reversal of crosslink was applied to both input and unsheared chromatin. First, 150 µl TE buffer was added to complete to 200 µl. Then, 4 µl RNAse A

(10mg/ml) was added and incubated for 30 minutes at 37°C. After the incubation, 20 µl %10 SDS, 4 µl 5M NaCl and 2 µl Proteinase K (20mg/ml) was added and incubated at 55°C for at least 2.5 hours then at 65°C overnight. In the following morning, the tube was centrifuged for 10 minutes at max speed. Then, Zymo DNA Clean & Concentrator Kit was used for DNA elution. Unsheared and input chromatin was loaded on %1.7 agarose gel to check if sonication was successful (between 200-500 bp).

Immunoprecipitation step:

For pre-blocking of magnetic beads, 60 µl magnetic beads were added to a 1.5 ml Eppendorf. 1 ml TE (pH = 8.0) was added and mixed by inverting. Then, Eppendorf was placed on a magnetic stand and waited 1 minute before discarding the solution. This step was repeated. tRNA was incubated for 5 minutes at 95°C for denaturation. Beads were resuspended with 100 µl TE, 10 µl BSA (10 mg/ml) and 10 µl tRNA (10 mg/ml). Then beads were incubated at 4°C for 2 hours overhead shaking. After that, beads were washed 3 times with 1 ml TE. Finally, 60 µl TE was added and kept at 4°C.

For pre-clearing of the chromatin, 10 µl of blocked magnetic beads were added to fragmented chromatin and incubated for 1 hour at 4°C. Supernatant was collected on magnetic stand. For immunoprecipitation step, 4 µl H3K4me3 antibody was added to the fragmented chromatin and incubated overnight at 4°C overnight shaking. In the following morning, 50 µl of pre-blocked magnetic beads were added on fragmented chromatin and incubated for 3 hours at 4°C overhead shaking. Then supernatant was discarded on magnetic stand. Chromatin magnetic beads mix was resuspended in PIC containing 1 ml Lysis buffer and incubated for 5 minutes at RT overhead shaking. Supernatant was discarded on magnetic stand. Then washing step with Lysis buffer was repeated. After that, chromatin solution was washed with PIC containing 1 ml DOC buffer and then washed with PIC containing 1 ml TE buffer. Supernatant

was discarded. Washed chromatin was spun for 3 minutes at 960g 4°C and supernatant was removed.

For elution of chromatin, beads were resuspended in 100 µl elution buffer and incubated for 15 minutes at 25°C 1000 rpm on shaker (vortexed briefly every few minutes). Then it was spun for 2 minutes at 11000 rpm RT and supernatant was collected. This step was repeated one more time. Then reversal of crosslink for IP fraction was performed. 4 µl RNase A was added and incubated for 30 minutes at 37°C. Then 4 µl 0.5M EDTA, 8 µl 1M Tris (pH=6.5) and 0.5 µl Proteinase K were added and incubated at 55°C for at least 2.5 hours and then at 65°C overnight. In the following morning, DNA was eluted with Zymo DNA Clean & Concentrator Kit as before.

#### *3.5.1.6.1. ChIP Real-Time PCR*

To verify if the ChIP experiment is worked, ChIP-qPCR was used. Positive and negative genes were determined according to the previous ChIP-seq data of our lab. FastStart Essential DNA Green Master Kit protocol was followed. Input DNAs were diluted 1/20, ChIP DNAs were diluted 1/4. For each reaction, 5 µl FastStart Essential DNA Green Master, 2 µl PCR grade water, 0.5 µl of each primer, 2 µl DNA were mixed. qPCR 96-well plates were read with Applied Biosystems 7500 Fast real-time PCR system. Real-time PCR conditions were as follows. Initial denaturation at 95°C for 10 minutes, 40 cycles of denaturation at 95°C for 10 seconds, annealing at 60°C for 20 seconds and extension at 72°C for 30 seconds, final extension at 68°C for 5 minutes. For melting step, 95°C for 10 seconds, 65°C for 60 seconds and 97°C for 1 second.

#### *3.5.1.6.2. ChIP Library Preparation and Next Generation Sequencing*

Library preparation and next generation sequencing of the ChIP samples were done by European Molecular Biology Laboratories (EMBL)

Genomics Core Facility as service procurement. Library preparation was done with NEBNext DNA Ultra II Kit. Sequencing was done with NextSeq500 device and parameters were set as 75SE (single end) high output mode.

#### *3.5.1.7. Generating KDM6A Q555* Mutation and Cloning to a Lentiviral Vector*

Complete KDM6A gene was retrieved from pCMV-HA-UTX plasmid. In according to do that, double digestion protocol was applied as follows. For double digestion, NotI and KpnI restriction enzymes were used. First, 1 µg pCMV-HA-UTX plasmid DNA, 1 µl NotI-HF, 1µl KpnI-HF restriction enzymes, 5 µl 10X CutSmart Buffer were mixed and completed to 50 µl with $ddH_2O$ for double digestion reaction and incubated for 1 hour at 37°C to extract complete KDM6A gene sequence. Then, digested plasmid mix was loaded to %1 agarose gel. After that, KDM6A gene and plasmid backbone were extracted with PCR clean-up gel extraction kit. To establish Q555* mutation (c.1663C>T), Q555_F_1 and Q555_S1_R primers from Table 20 were used for two-step conventional PCR reaction. 9 ng KDM6A DNA, 12.5 µl OneTaq ® Hot Start Quick-Load ® 2X Master Mix, 0.5 µl of each plasmid were mixed and completed to 25 µl with $ddH_2O$. Two-step conventional PCR conditions were as follows. Initial denaturation at 94°C for 30 seconds, 30 cycles of denaturation at 94°C for 30 seconds and annealing + extension at 68°C for 3 minutes, final extension at 68°C for 5 minutes. After that, 7.5 µl of PCR product was loaded to %1.5 agarose gel to check if the size of the amplified DNA is as expected (1700 bp). To check whether the mutation was established properly some of the PCR product was sent to Sanger Sequencing with universal mCherry-F and WPRE-R primers after PCR clean up with PCR clean-up gel extraction kit.

Double digestion was applied to mutated KDM6A DNA with KpnI and NotI as mentioned above. Ligation reaction was set with plasmid backbone as follows. 50 ng pCMV-HA-UTX empty backbone, 40 ng mutated KDM6A DNA,

0.5 µl T4 ligase, 1 µl T4 ligation buffer were mixed and completed to 10 µl with $ddH_2O$ and incubated at RT for 2 hours. Negative ligation controls were also prepared with no ligase and no insert. Transformation of ligated products to 10 beta bacteria and colony PCR were applied as mentioned in section 3.5.1.2.3. The colonies with positive gel band were grown and DNA was isolated with Mini Plasmid DNA Purification kit. Mutated KDM6A containing plasmid was sent to Sanger Sequencing for validation.

HEK293T cells were transfected with uncut pCMV-HA-UTX and mutated KDM6A plasmids was applied to see if the short form of the KDM6A protein was translated. Western blot protocol was applied according to method described in section 3.5.1.4.

To clone the mutated KDM6A DNA to pUltra-hot 3$^{rd}$ generation lentiviral vector, double digestion reaction was set for both pUltra-hot and pCMV-HA-UTX separately. Double digestion with Q555* mutated KDM6A containing pCMV-HA-UTX was applied as follows: 1 µl Nhe-HF, 1 µl XhoI, 5 µl 10X CutSmart buffer, 1 µg KDM6A mutated pCMV-HA-UTX plasmid was mixed and completed to 50 µl with $ddH_2O$. Double digestion with pUltra-hot lentiviral vector was applied as follows: 1 µl NheI-HF, 1 µl SalI-HF, 5 µl 10X CutSmart buffer, 1 µg pUltra-hot were mixed and completed to 50 µl with $ddH_2O$. Both reactions were incubated at 37°C for 2 hours. Then, samples were loaded to %1 agarose gel and run at 100V for 45 minutes. pUltra-hot backbone (7000 bp) and mutated KDM6A insert (1700 bp) were extracted from the gel and isolated. Ligation reaction was applied as follows. 50 ng pUltra-hot backbone, 35.4 ng mutated KDM6A insert, 0.5 µl T4 ligase, 1 µl 10X T4 ligation buffer were mixed and completed to 10 µl with $ddH_2O$ and incubated at RT for 2 hours. Negative ligation controls were also prepared with no ligase and no insert. Transformation of ligated products to Stbl3 bacteria and colony PCR were applied as m described in methods section 3.5.1.2.3. The colonies with positive gel band were grown and its DNA was isolated with Mini Plasmid DNA

Purification kit. Mutated KDM6A containing pUltra-hot lentiviral vector was sent to Sanger Sequencing for validation.

### *3.5.2 Computational Methods*

#### *3.5.2.1. Data Acquisition and Preprocessing*

##### *3.5.2.1.1. ATAC-seq Data*

Bladder cancer ATAC-seq peaks (n=10) and normalized ATAC-seq signal of the respective peaks (5) were obtained from the TCGA Publication Page link (https://gdc.cancer.gov/about-data/publications/ATACseq-AWG ).

##### *3.5.2.1.2. DNA Methylation Data*

TCGA-BLCA 450k DNA Methylation data from (4) was used. 412 bladder cancer patients' normalized DNA methylation beta values have been obtained via "TCGAbiolinks" R Bioconductor package.

##### *3.5.2.1.3. Gene Expression Data*

"TCGAbiolinks" R Bioconductor package available for 408 bladder cancer patients was used to obtain gene expression data from Robertson2017. For gene expression analysis, FPKM-UQ data was used and Log2 normalization was applied to the data.

Gene expression data from (58) was obtained via "consensusMIBC" R package (42). Robust Multichip Average (RMA) data was used for gene expression analysis.

Gene expression data from (59) was obtained via cBioPortal database. Quantile Normalization (QN) data was used for gene expression analysis.

Mean expression values of the genes for neuronal and non-neuronal subgroups within each cohort were calculated and used for ß-catenin target gene expression analysis and visualization.

#### *3.5.2.1.4. ChIP-seq Data*

ChIP-seq data generated with next generation sequencing was downloaded from EMBL Faspex system as ‘fastq’ files. Alignment was processed with ‘chipseq’ pipeline generated by nf-core (60). To summarize the pipeline, first ‘fastQC’ tool used for quality control step. Then, ‘Cutadapt’ tool was used for trimming adapter sequences. After that, alignment is done with ‘BWA’ alignment tool. Then, ‘Picard’ command line tools were used to mark duplicates. Finally, ‘SAMtools’ was used to generate compact BAM files.

Peak calling was applied using MACS tool (61). ‘callpeak’ function of MACS2 was used and the parameters were set as follows. P value cutoff = $10^{-5}$, q value (minimum FDR) cutoff = 0.1, fragment size = 200bp and ‘broad’ arguments were used.

We kept the peaks which are located within ±3 kb distance to transcriptional start sites (TSS) of the genes. After this step, most enriched 500 peaks were identified according to their peak scores. Then, enrichment analysis was applied to the genes corresponding to these peaks using R “pathfindR” package (62).

### *3.5.2.2. Data Analysis and Integration*

#### *3.5.2.2.1. ATAC-seq Data Analysis and Clustering*

Bladder cancer ATAC-seq signals at all the MIBC ATAC-seq peaks (n=107,921) were averaged between the replicates of the ATAC-seq MIBC cohort (n=10). “sd” function -which calculates the standard deviation among given numbers- was applied to the data by using R programming language to acquire the most variable 20,000 ATAC-seq peaks. “kmeans” function of the “stats” package of R was used to cluster the retained peaks. Clustering was performed by using k means with k=3, empirically chosen such that the analysis resulted in distinct clusters consisting of comparable regulatory

elements. Annotations of the MIBC were done according to the mRNA subgroup definitions from TCGA study

#### *3.5.2.2.2. Integration with DNA Methylation Data*

As DNA methylation beta-values were based on hg19 assembly, the coordinates of the regulatory clusters were lifted to hg19 using USCS liftOver tool (63). Hence, 4854 (cluster 1), 8035 (cluster 2), 7028 (cluster 3) regulatory regions were retained for further analysis. Afterwards, for each of the regulatory clusters (neuronal, non-neuronal and luminal outlier), genomic coordinates of the respective regulatory cluster were overlapped with the 450k CpG coordinates using “GenomicRanges” R Bioconductor package. Neuronal cluster, non-neuronal cluster and luminal outlier clusters were overlapped 1229, 3846 and 1667 CpG sites, respectively. Then, average DNA methylation levels for each MIBC tumor (n = 412) were determined by calculating the average beta-value at the CpG sites overlapping with the respective regulatory cluster. For each regulatory cluster, average beta-values were represented as boxplots according to the molecular subgroup annotations (4). ANOVA and post hoc analyses were used to examine the variations in DNA methylation levels among the subgroups statistically.

#### *3.5.2.2.3. Identification of Target Genes of MIBC Subgroup Specific Active Regulatory Regions*

Target genes of the three regulatory clusters were identified by matching peak IDs with the ones available in Supplementary Table 7 from (5) which provides pan-cancer peak ids, their genomic coordinates, and their linked target genes.

#### *3.5.2.2.4. GO Term and Pathway Analysis*

For GO term and pathway analysis, “clusterProfiler” (64) R Bioconductor package was used Only terms with an FDR of less than 0.05

were included in the KEGG pathway and GO term analyses. GO term analysis was performed for only 'biological process'. "pathfindR" R package was used for Reactome pathway analysis (62).

#### *3.5.2.2.5. Transcription Factor Analysis*

The online database Enrichr (65, 66) with the 'transcription ChEA' option was utilized to investigate which transcription factors are involved in the regulation of neural regulatory element-targeted genes.

Transcription factor motif finding analysis was performed via HOMER motif finding algorithm (67) using the "findMotifsGenome.pl" command with -size given and hg38 options.

#### *3.5.2.2.6. Mutation Analysis*

For mutation analysis of bladder cancer patients (4), cBioPortal database was used. ß-catenin and the genes which are the members of ß-catenin destruction complex were investigated for their mutation rate for both neuronal and non-neuronal samples. To see the effects of these mutations on proteins, DANN, SIFT and PROVEAN scores were used. MutationTaster database was used to predict how the mutation affects the protein's function.

### *3.5.2.3. Data Visualization*

#### *3.5.2.3.1. Heatmap Representations*

ATAC-seq signal of the clusters defined by k-means was visualized using 'pheatmap' function of pheatmap R package (68).

#### *3.5.2.3.2. Boxplot and Dotplot Representations*

To represent boxplots, R “boxplot” function was used. For visualization of the pathway enrichment analysis, “dotplot” function of “enrichplot” R package (69) was used. “enrichment_chart” function of the “pathfindR” R package was used to visualize Reactome pathway results (62).

#### *3.5.2.3.3. Snapshot Representations*

USCC Xena browser (70) was used to visualize the data all for ATAC-seq, DNA methylation and gene expression available for 10 samples. ATAC-seq peak regions and the specific gene regions that are linked to those peak regions were visualized.

#### *3.5.2.3.4. Oncoprint Images*

Oncoprint images to represent the mutation rates in ß-catenin and ß-catenin destruction complex components were generated via https://www.cbioportal.org.

### 3.6. Study Plan

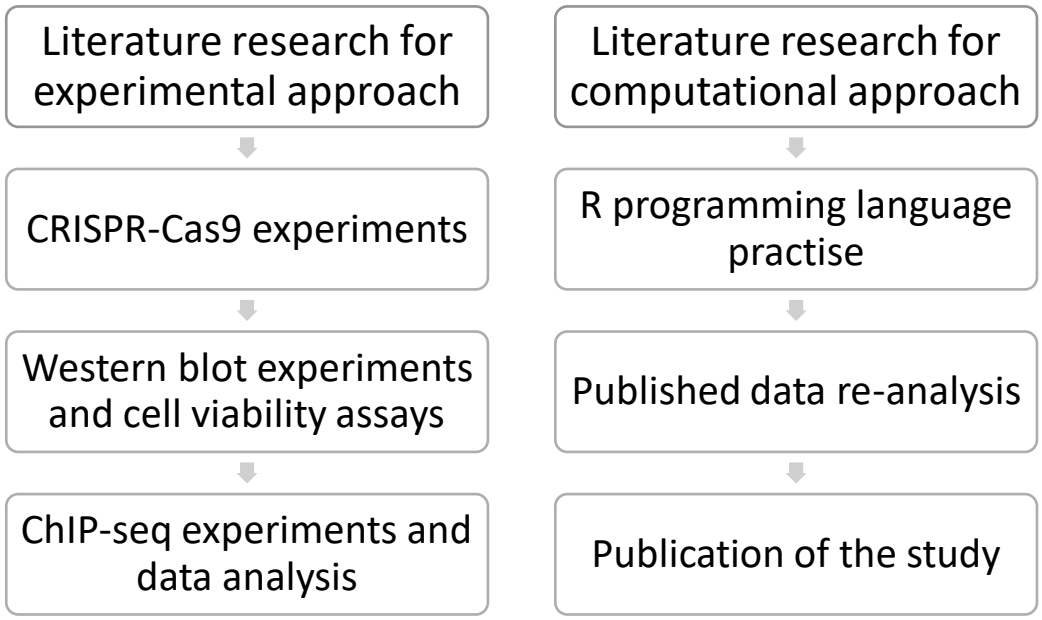

### 3.7. Evaluation of Data

Statistical analyses were done using R/Bioconductor packages (**www.bioconductor.org**). In boxplot comparisons ANOVA test was used. Post hoc tests after ANOVA was performed using “PostHocTest” function of “DescTools” R package (71). For correlation analyses Wilcoxon rank sum test was used. Significance threshold was set as p value < 0.05. To see the enrichment pattern of ß-catenin in neuronal subtype versus non-neuronal bladder cancer, Fisher’s Exact test was used.

### 3.8. Limitations of the Study

There were no limitations of the study.

### 3.9. Ethics Committee Approval

This study was approved by the Izmir Biomedicine and Genome Center Non-Interventional Research Ethics Committee (IBG-GOEK) on 28.04.2020. Ethics committee approval protocol number is 2020-018.

# 4. RESULTS

## 4.1. Analysis of open chromatin regions in muscle invasive bladder cancer

ATAC-seq data (5) for chromatin accessible regions of bladder cancer samples was re-analyzed and clustered (Figure 8).

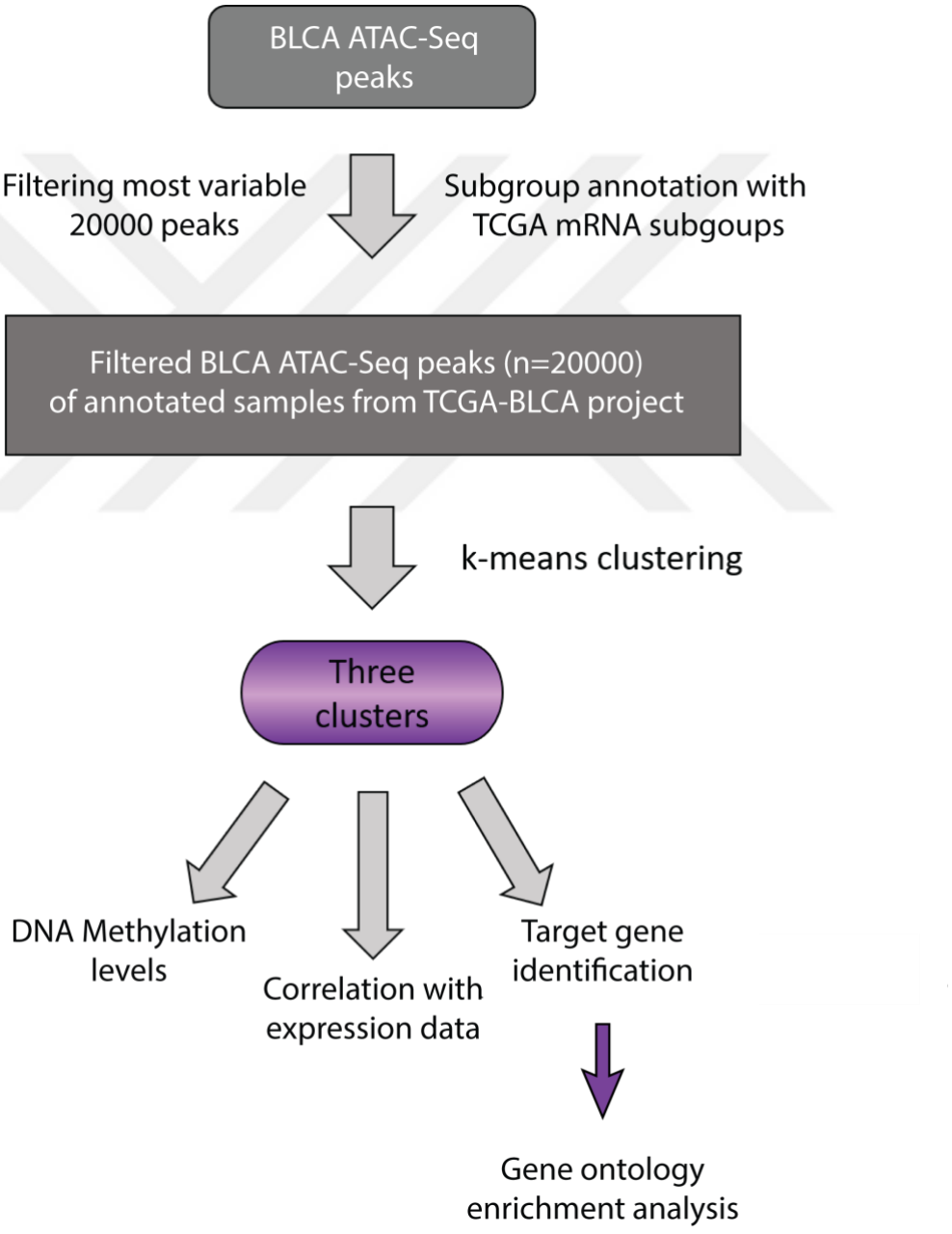


*Figure 8. Flowchart of data processing and integrative data analysis.*

### *4.1.1. Subgroup specific regulatory regions of MIBC*

Three bladder regulatory regions were defined by using subgroup specific annotations from latest TCGA study (4) which termed as neuronal (n=4868), non-neuronal (n=8067) and luminal outlier (n=7065) (Figure 9a). DNA methylation levels on the identified clusters were computed using 450k DNA methylation data available for 412 bladder cancer patients to determine the subgroup specificity of the defined regulatory regions. The neuronal molecular subtype of bladder cancer patients had lowest DNA methylation levels at the neuronal regulatory regions (p value = 1.91e07). For the non-neuronal regulatory regions, neuronal subtype was significantly hypermethylated compared to other subtypes (p value < 2e−16) (Figure 9b). DNA methylation levels for the molecular subtypes in the luminal outlier cluster were varied (Figure 10a). When the DNA methylation level of the outlier luminal papillary sample (TCGA-GC-A3JW) was compared to the other 4 luminal papillary samples included in the clustering analysis, it was discovered that the outlier sample had significantly lower DNA methylation levels at luminal outlier regulatory elements than the other luminal papillary samples (Figure 10b). These findings suggest that bladder cancer regulatory region classifications were in accordance with the DNA methylation landscape of the respective regions, implying that lower DNA methylation levels were identified for a molecular subgroup at active regulatory elements belonging to the same subgroup across the entire TCGA cohort (n = 412).

Once the regulatory elements were defined, one of the key questions was to link the regulatory elements with their target genes. Although several strategies have been employed to address this question, it appeared that identification of the target genes based on correlation of regulatory region signal activity and expression level of genes gave very reliable results (72, 73). Corces et al. followed a similar strategy to define the target genes of DNA regulatory elements they defined pan-cancer. Three regulatory clusters that were established for bladder cancer were associated to target genes to discover the genes and pathways

differentially implicated for the three clusters (Figure 9). 117 target genes for neuronal cluster, 371 target genes for non-neuronal cluster, and 107 target genes for luminal outlier cluster were identified using this method.

Target genes of the neuronal cluster were exclusively involved in WNT signaling and its regulation (Figure 9c). Performing a GO term enrichment analysis for the non-neuronal cluster target genes was revealed an enrichment for the terms epithelial differentiation and epidermis development, suggesting divergence of non-neuronal bladder cancer from the neuronal ones mainly by epithelial characteristics (Figure 9d). Although significantly implicated gene ontology biological process could not be identified for the luminal outlier cluster, performing a KEGG pathway analysis for this cluster was showed an enrichment for Drug Metabolism and Chemical Carcinogenesis Pathways (Figure 10c). Following this discovery and a review of the available clinical data, this outlier patient was given a combination of carboplatin and Gemzar chemotherapy (4). Only 2 of the other 9 bladder cancer patients had accessible clinical data, and both treated with Gemcitabine (Gemzar) and Cisplatin therapy, indicating that Carboplatin treatment may have an impact on the differential regulatory landscape of this outlier sample belonging to the luminal subtype group. However, this result should be interpreted with caution because of the lack of sufficient data.

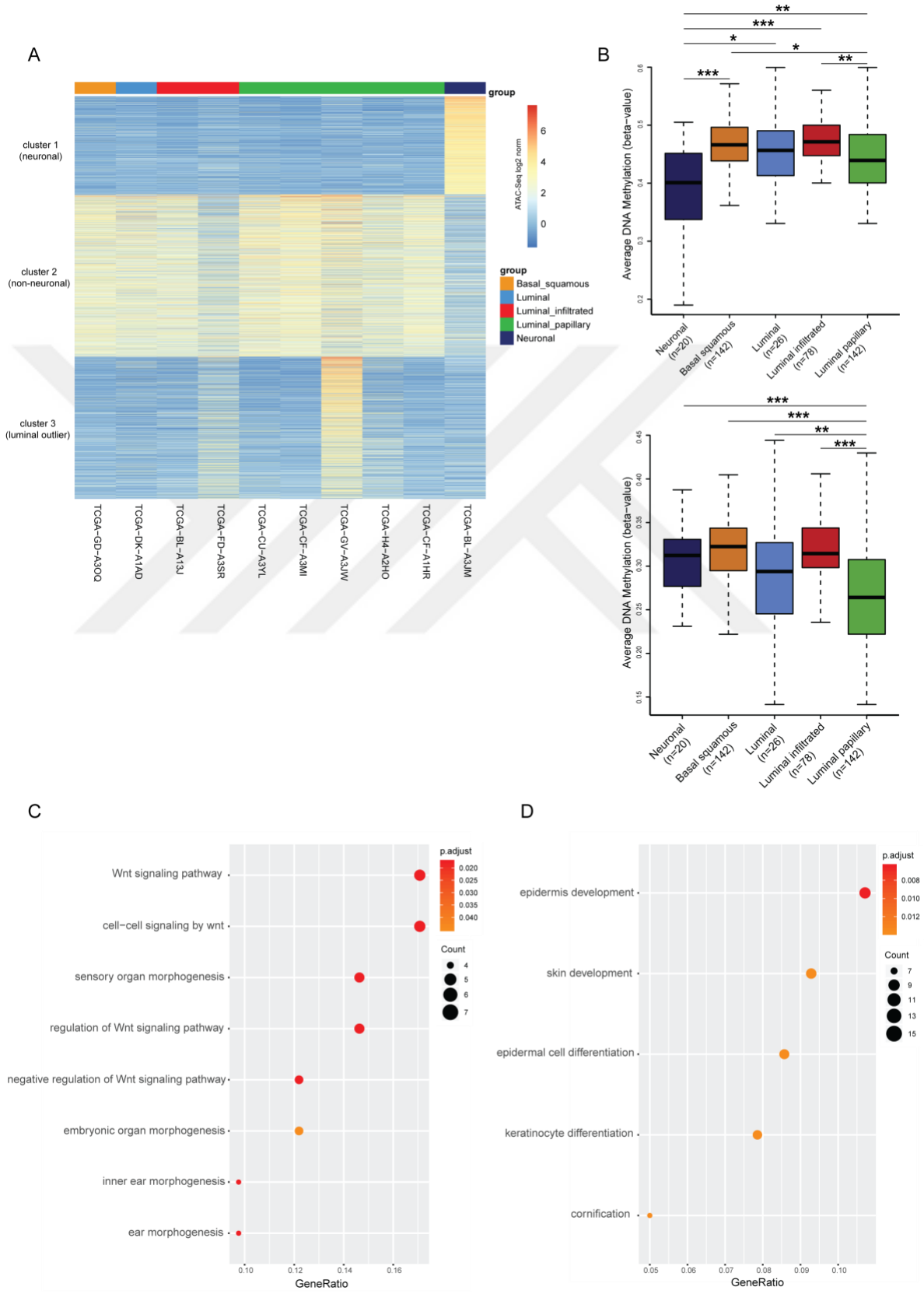
A
group
cluster 1
(neuronal)
cluster 2
(non-neuronal)
cluster 3
(luminal outlier)
ATAC-Seq log2 norm
6
4
2
0
group
Basal_squamous
Luminal
Luminal_infiltrated
Luminal_papillary
Neuronal
TCGA-GD-A3OQ
TCGA-DK-A1AD
TCGA-BL-A13J
TCGA-FD-A3SR
TCGA-CU-A3YL
TCGA-CF-A3MI
TCGA-GV-A3JW
TCGA-H4-A2HO
TCGA-CF-A1HR
TCGA-BL-A3JM
B
Average DNA Methylation (beta-value)
Neuronal (n=20)
Basal squamous (n=142)
Luminal (n=26)
Luminal infiltrated (n=78)
Luminal papillary (n=142)
C
Wnt signaling pathway
cell-cell signaling by wnt
sensory organ morphogenesis
regulation of Wnt signaling pathway
negative regulation of Wnt signaling pathway
embryonic organ morphogenesis
inner ear morphogenesis
ear morphogenesis
p.adjust
Count
GeneRatio
D
epidermis development
skin development
epidermal cell differentiation
keratinocyte differentiation
cornification
p.adjust
Count
GeneRatio

*Figure 9. Subgroup specific regulatory regions of bladder cancer. (a) Heatmap visualization of the k-means clustering of most variable bladder cancer ATAC-seq peaks. Three clusters were represented; cluster 1: neuronal, cluster 2: non-neuronal and cluster 3: luminal outlier. (b) DNA methylation levels (Beta values) of mRNA subgroups on the regulatory regions: cluster 1 (upper panel) (Anova p value = 1.91e−07) and cluster 2 (lower panel) (Anova p value < 2e−16). PostHocTest significance codes: *p < 0.05; **p < 0.01; ***p < 0.001. (c,d) Gene Ontology terms enriched for the target genes of cluster 1 (c) and cluster 2 (d). The dotplot was generated using "clusterProfiler" R/Bioconductor package. Dot sizes indicating gene counts of specific terms.*

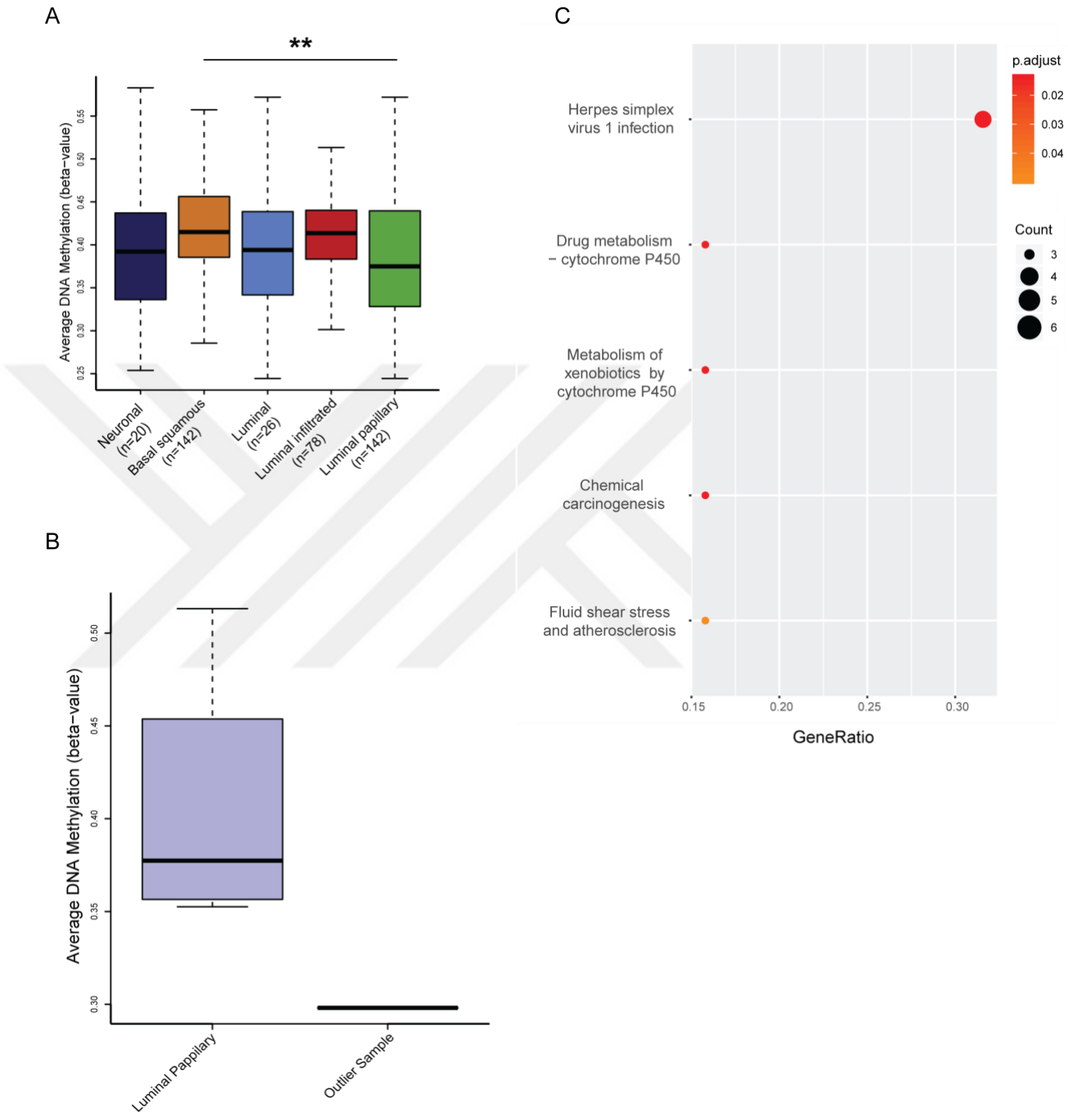


*Figure 10. Analysis of the DNA methylation levels and KEGG pathway analysis for the target genes of the luminal outlier regulatory elements. (a) Boxplot shows the DNA methylation levels (Beta values) of mRNA subgroups at the luminal outlier regulatory regions (cluster 3) (*p<0.05; **p<0.01; ***p<0.001). (b) Boxplot displays the DNA methylation levels of luminal outlier sample (n=1) and other luminal*

*papillary samples (n=4) at the cluster 3 regulatory regions. (c) Dot sizes indicating gene counts of specific terms.*

### *4.1.2. Neuronal active regulatory regions are targeted by ß-catenin and TCF/LEF*

Initially, performing an analysis via EnrichR program was significantly associated the target genes of the neuronal regulatory elements with ß-catenin targets (p value = 3.59e−08) (Figure 11a). After that, all neuronal specific regulatory elements (Figure 9a, neuronal cluster) were subjected to an unbiased transcription factor motif enrichment analysis, regardless of their relationship with a gene target. Remarkably, this analysis was identified the TCF/LEF binding motifs as the top enriched motifs in both de novo and known motif finding modes of the HOMER algorithm (67) (Figure 11b, c). In contrast, there was no enrichment for the TCF/LEF motif in non-neuronal regulatory regions when transcription factor motif analysis was performed (Data not shown). The major downstream factors of WNT signaling in the nucleus are TCF/LEF transcription factors, which bind ß-catenin directly and regulate the expression of target genes (74, 75). ß-catenin itself does not have a binding motif available in the HOMER algorithm as it is a transcriptional co-activator (76, 77). However, having identified the motifs of TCF/LEF, which can directly bind ß-catenin, directly at neuronal regulatory elements highly argues for the regulation of neuronal regulatory regions by ß-catenin-TCF/LEF complex.

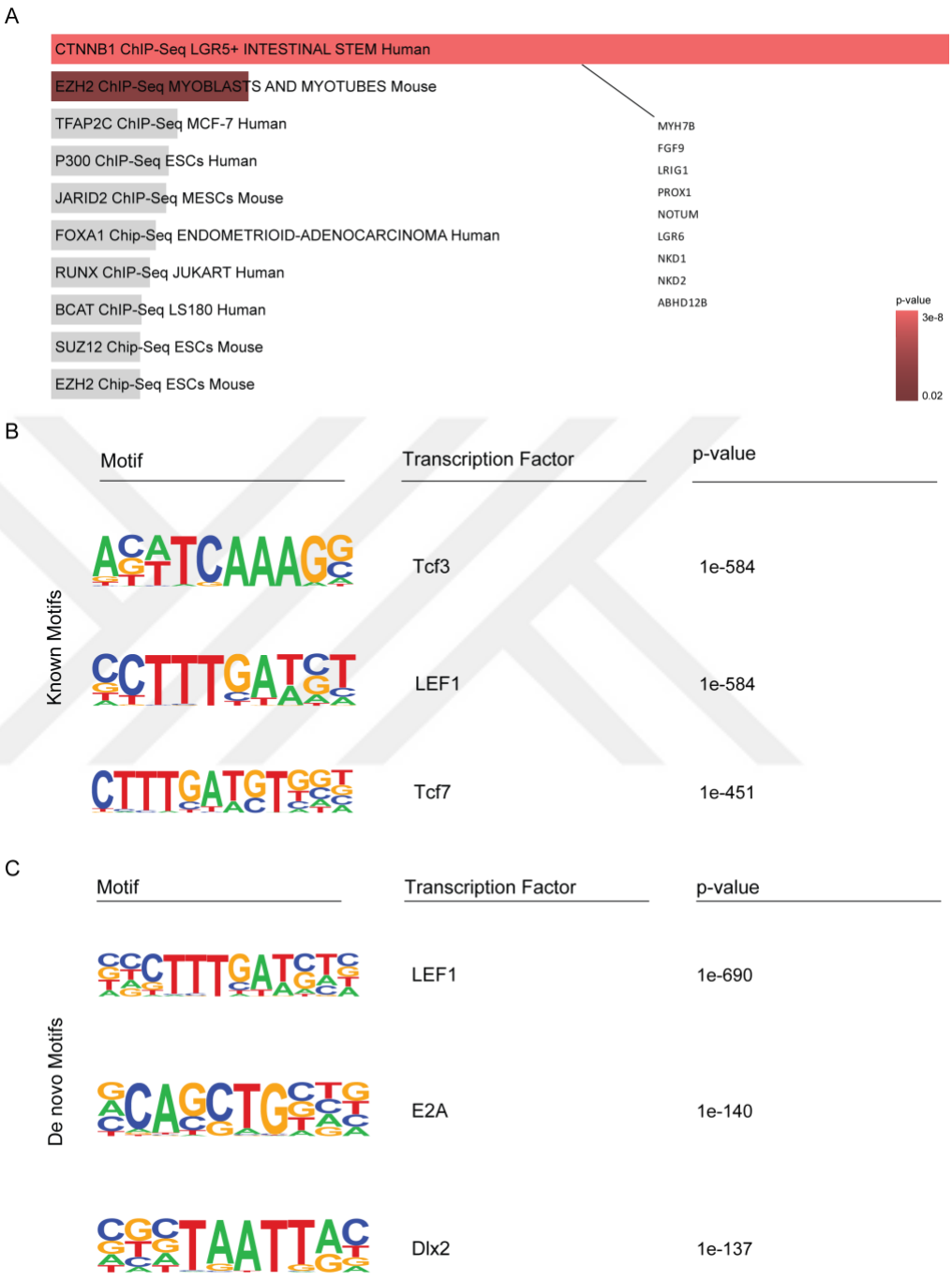


*Figure 11. Transcription factor motif analysis for the neuronal regulatory elements. (a) ChEA factor analysis using the program EnrichR for the target genes of the neuronal regulatory elements (p value = 3.59e−08). (b) HOMER known transcription factor motif analysis at the neuronal regulatory regions. Top three*

*enriched motifs are displayed. (c) HOMER de novo transcription factor motif analysis at the neuronal regulatory regions. Top three enriched motifs and best matched transcription factors are displayed.*

### *4.1.3. Overexpression of neuronal regulatory element target genes regulated by ß-catenin in neuronal subtype of bladder cancer*

As the transcription factor analysis associated ß-catenin-TCF/LEF factors with neuronal regulatory regions, the (epi)genomic and transcriptomic profiles of ß-catenin targets were analyzed in more detail. Hypomethylation was discovered at the regulatory element targeting the NKD1 gene, which is a negative regulator of WNT signaling and has increased expression in various malignancies with aberrant WNT signaling (78). Furthermore, analyzing the gene expression data available for 408 samples, NKD1 was significantly upregulated in neuronal subtype (p value = 2.33e−16) (Figure 12a). Similarly, checking the (epi)genomic profiles at FGF9 locus, highly implicated in neuronal differentiation (79, 80) showed the hypomethylation directly at the regulatory element targeting this gene, with significantly increased patterns of expression in the neuronal subtype (Figure 12b). The expression patterns of all genes that were targets of ß-catenin and regulated by neuronal regulatory elements indicated that neuronal subtype had considerably higher expression than other subtypes (Figure 12c). In the recent study carried out by (42) and colleagues, 1750 bladder cancer transcriptome were analyzed and molecular subtypes for these samples were annotated. One of the molecular subtypes identified in this study was referred to as "neuroendocrine-like". The transcriptome data from the additional two cohorts included in (42) were accessed and the expression profiles of β-catenin target genes regulated by neuronal active regulatory elements that identified in this study were analyzed. In these two additional cohorts, the same set of genes were shown to be substantially upregulated in neuroendocrine-like bladder cancer (Figure 12d,e), in line with our findings with the TCGA cohort. Therefore, in neural subtype bladder cancer, our

findings point out to upregulation of genes implicated in WNT signaling via activation of ß-catenin.

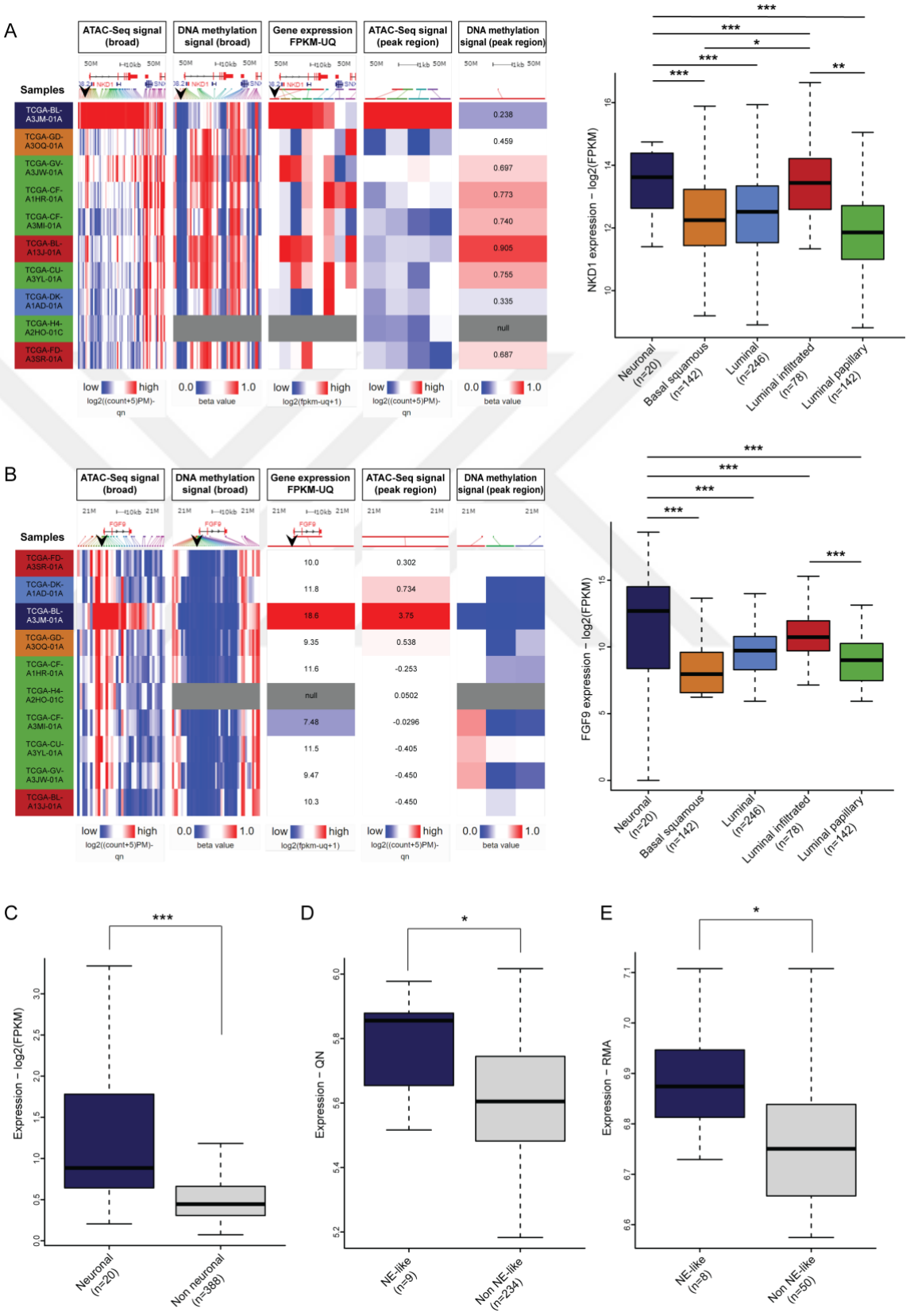
A
ATAC-Seq signal (broad)
DNA methylation signal (broad)
Gene expression FPKM-UQ
ATAC-Seq signal (peak region)
DNA methylation signal (peak region)
Samples
TCGA-BL-A3JM-01A
TCGA-GD-A3OQ-01A
TCGA-GV-A3JW-01A
TCGA-CF-A1HR-01A
TCGA-CF-A3MI-01A
TCGA-BL-A13J-01A
TCGA-CU-A3YL-01A
TCGA-DK-A1AD-01A
TCGA-H4-A2HO-01C
TCGA-FD-A3SR-01A
0.238
0.459
0.697
0.773
0.740
0.905
0.755
0.335
null
0.687
low high
log2((count+5)PM)-qn
0.0 1.0
beta value
log2(fpkm-uq+1)
NKD1 expression – log2(FPKM)
Neuronal (n=20)
Basal squamous (n=142)
Luminal (n=246)
Luminal infiltrated (n=78)
Luminal papillary (n=142)
B
FGF9
10.0
11.8
18.6
9.35
11.6
null
7.48
11.5
9.47
10.3
0.302
0.734
3.75
0.538
-0.253
0.0502
-0.0296
-0.405
-0.450
-0.450
FGF9 expression – log2(FPKM)
C
Expression – log2(FPKM)
Neuronal (n=20)
Non neuronal (n=388)
D
Expression – QN
NE-like (n=9)
Non NE-like (n=234)
E
Expression – RMA
NE-like (n=8)
Non NE-like (n=50)

*Figure 12. (Epi)genomic profiles of ß-catenin target genes regulated by neuronal regulatory regions. a-b Xena Browser snapshots show the ATAC-seq, DNA methylation and gene expression profiles for the bladder cancer patients (n = 10) at NKD1 (a) (Anova p value = 2.33e-16) and FGF9 loci (b) (Anova p value < 2e−16). PostHocTest significance codes: *p < 0.05; **p < 0.01; ***p < 0.001. Regions marked by blue arrows indicate the neuronal regulatory element regulating the respective genes. In the snapshots left, the last two panels show the ATAC-seq and DNA methylation signals directly at the regulatory elements marked with the blue arrows. Boxplots next to the snapshots show the expression levels of NKD1 and FGF9 across the bladder cancer subgroups. (c–e) Expression of all ß-catenin target genes regulated by neuronal regulatory elements between neuronal and non-neuronal subgroups of bladder cancer belonging to TCGA cohort (4) (c) (Wilcoxon rank sum test p value = 9.807e−07) and Neuroendocrine like (NE-like) and non NE-like bladder cancers (42) belonging to the cohorts Sjödahl (58) (d) (Wilcoxon rank sum test p value = 0.01959), Iyer (59) (e) (Wilcoxon rank sum test p value = 0.0127) respectively. (*p < 0.05; **p < 0.01; ***p < 0.001).*

### *4.1.4. Correlation of ß-catenin target genes and N-cadherin expressions*

The decrease of E-cadherin expression and the rise of N-cadherin expression, referred to as "cadherin switching," are well-known markers of cancer's epithelial to mesenchymal transformation (81). Hence, N-cadherin expression has previously been demonstrated to be a prognostic marker in bladder cancer, with the greatest levels of expression found in T2 and T3 tumors. (82). Comparing the expression levels of N-cadherin and E-cadherin revealed significantly higher expression of N-cadherin and significantly lower expression of E-cadherin in neuronal bladder cancer compared to non-neuronal samples (Figure 13a,b). WNT signaling is also known to promote the expression of N-cadherin while suppressing the expression of E-cadherin (83). In the samples belonging to the neuronal subtype, there were strong correlations between N-cadherin expression and expression of ß-catenin target genes regulated by neuronal specific regulatory

elements and related to neurogenesis (Figure 9a), such as FGF9 and PROX1 (Figure 13c). Overall, our findings show that increased N-cadherin expression is linked to ß-catenin/WNT signaling activation in neural bladder cancer, potentially affecting this subtype's invasive characteristics.

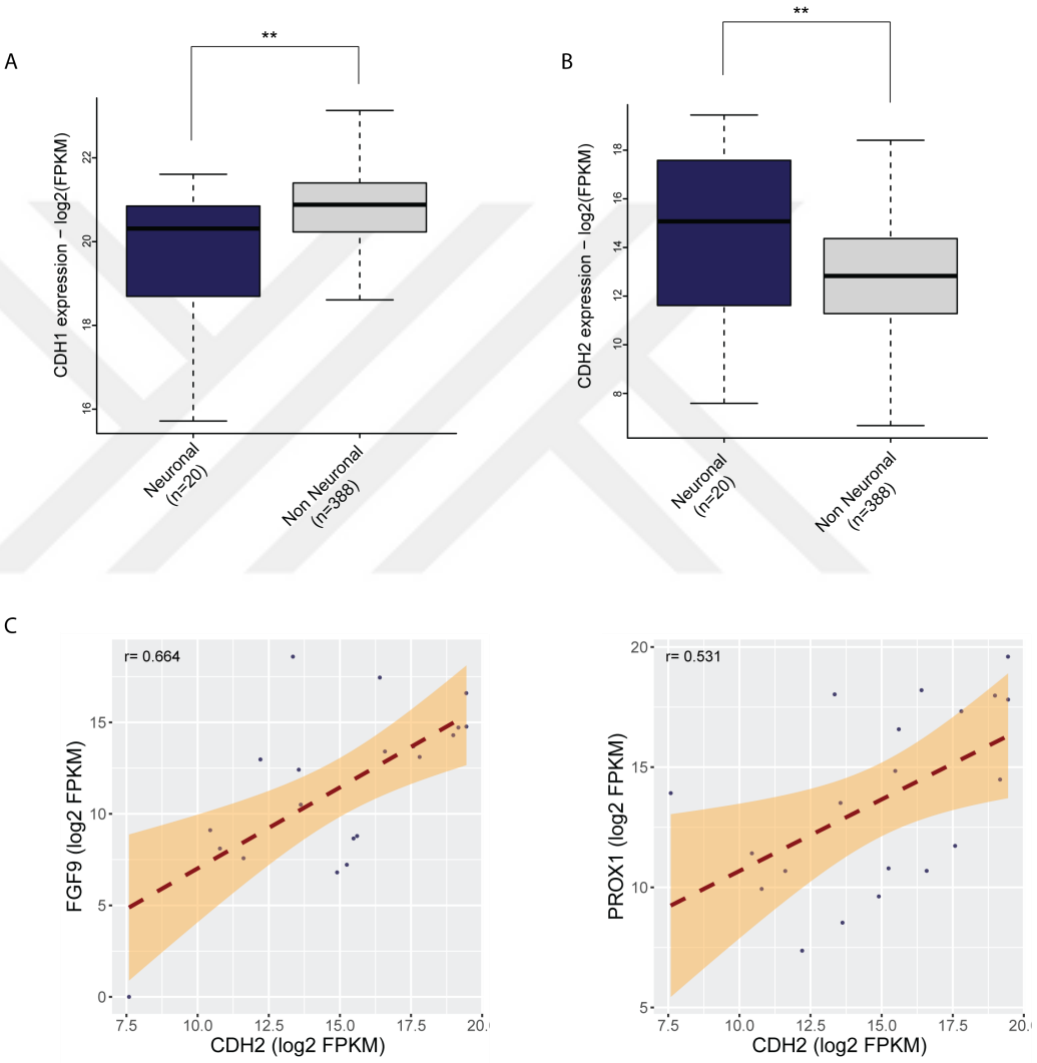


*Figure 13. Expression of cadherins and their relation to ß-catenin target gene expression. a-b Boxplots represent the expression of N-cadherin (a) (Wilcoxon rank sum test p value = 0.0083) and E-cadherin (b) (Wilcoxon rank sum test p value = 0.010) in neuronal and non-neuronal bladder cancer patients. (c) Scatter plots compare the expression of N-cadherin with the ß-catenin targets regulated by neuronal regulatory elements, FGF9 (Pearson correlation test p value = 0.001391)*

*and PROX1 (Pearson correlation test p value = 0.01583). (*p < 0.05; **p < 0.01; ***p < 0.001).*

### *4.1.5. Mutation levels of ß-catenin and ß-catenin destruction complex components in neuronal bladder cancer patients*

Since ß-catenin is a core downstream component of WNT signaling, its nuclear localization is tightly regulated by the ß-catenin destruction complex. In the absence of WNT, ß-catenin is phosphorylated and degraded by the destruction complex. However, in the presence of WNT, ß-catenin translocates to the nucleus and activates ß-catenin-TCF/LEF target genes (84) (Figure 14a). Since we identified neuronal regulatory regions to be associated with the ß-catenin-TCF/LEF complex, we questioned whether dysregulation of ß-catenin may influence the abnormal activation of WNT signaling in neuronal subtype of bladder cancer. Firstly, the mutation status of ß-catenin in all bladder cancer patients was investigated. The mutation rate of ß-catenin in neuronal samples was 20%, compared to 4.34 percent in non-neuronal samples, according to our findings. This result revealed a substantial rate of ß-catenin mutations in neural bladder cancer (Fisher's exact test p value = 0.0142) (Figure 14b), which was previously unknown. Exon 3 mutations in ß-catenin have previously been demonstrated to be oncogenic and cause nuclear accumulation of ß-catenin in the literature (54). After classifying ß-catenin mutations in all bladder cancer patients, we discovered an even stronger link between exon 3 ß-catenin mutations and the neuronal subtype (odds ratio = 31.33, p value = 1.786e-05) (Figure 14b,c). Importantly, all the ß-catenin mutations identified for neuronal samples were damaging and present in COSMIC database (85), and result in loss of phosphorylation sites, critical for the degradation of ß-catenin. Next, upon extending the mutation analysis for bladder cancer samples belonging to neuronal subtype for other proteins which are part of ß-catenin destruction complex (Figure 14a), cumulatively 55% of all neuronal samples had mutations in ß-catenin itself or in the destruction complex components (Figure

14d,e). Together, the findings clearly suggest that mutations in ß-catenin or its destruction complex components result in aberrant accumulation of ß-catenin in nucleus and activation of WNT signaling as a result of upregulation of ß-catenin target genes.

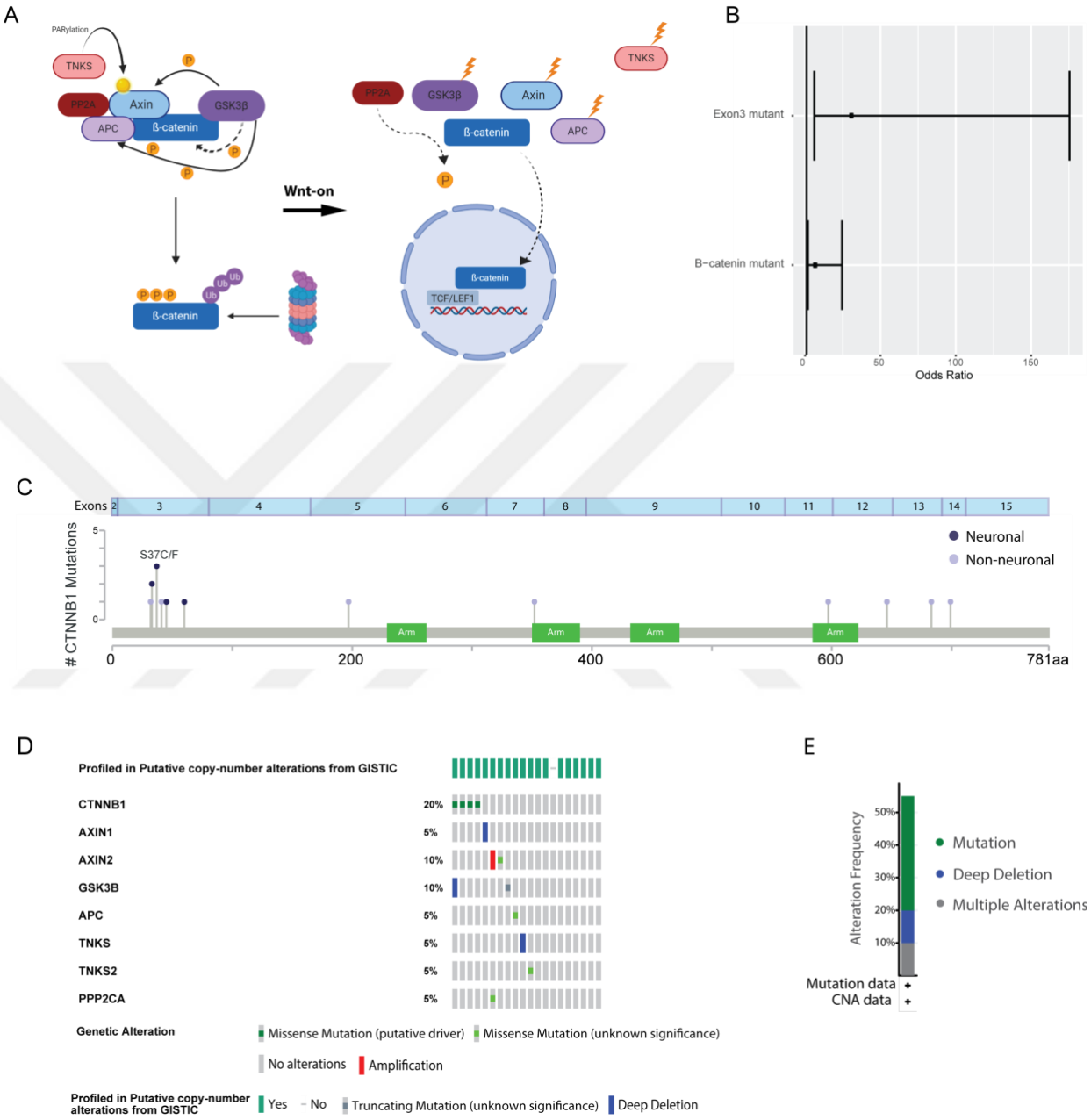


*Figure 14. Mutation profiles of ß-catenin and ß-catenin destruction complex components in bladder cancer patients. (a) Cartoon illustrating ß-catenin and ß-catenin destruction complex. (Created with BioRender.com) (b) Plots show the odds ratio (with 95% confidence interval) demonstrating the enrichment of all ß-catenin and exon 3 ß-catenin mutations in neuronal bladder cancer. (c) Lollipop plot showing the mutations of ß-catenin in bladder cancer (neuronal: dark blue and non-neuronal: gray).*

*(d) Oncoprint image displaying the mutation profile of ß-catenin and ß-catenin destruction complex components in samples belonging to the neuronal subtype. (e) Bar plot showing the cumulative mutation rate ß-catenin and ß-catenin destruction complex components.*

## 4.2. Role of KDM6A in epigenetic and phenotypic profile of 5637 bladder cancer cell line

### *4.2.1. KDM6A-null 5637*

#### *4.2.1.1. Generating KDM6A knock-out 5637 bladder cancer cell line via CRISPR-Cas9 method*

To generate *KDM6A* knock-out 5637 cells, three different gRNA were chosen from universal gRNA libraries. PX458 mammalian expression vector was used for knock-out experiments. gRNAs were successfully cloned into PX458 vector (Figure 5a). To transfect the 5637 cells with gRNA containing PX458, two different transfection reagent PEI (Polyethylenimine) and Lipofectamine were tested. Transfection with PEI reagent was resulted in many cell deaths that can be interpreted as toxic (Data not shown). Transfection with lipid-based reagent Lipofectamine was more efficient. Therefore, we decided to use Lipofectamine as transfection reagent. After transfection, GFP signal rates of the cells were below the expected (below %70). To generate single KDM6A knock-out colonies, transfected cells were sorted as single cells in 96-well plates. Colony numbers were lower than expected, however we were able to expand 6 different 5637 single colonies that were transfected with three different gRNAs (g43, g312 and Renilla g208) containing PX458. But CRISPR-Cas9 only worked for g312 single colonies (Figure 15b). For g43 single colonies, *KDM6A* gene was not knocked out since KDM6A protein signal was present at western blot results. However, g312 single clones did not show any signal at the expected size of KDM6A protein. Renilla g208 control gRNA single

colonies had signal at the size of KDM6A protein as expected. To further validate *KDM6A* knock-out, we sent the 5637 g312 sc1 (single clone 1) and sc2 (single clone 2) DNAs for Sanger sequencing. 5637 g312 sc1 sequencing quality was below the standards. However, 5637 g312 sc2 sequencing quality was good, so that we were able to analyze the sequencing results. Sanger sequencing was applied to both strands with two different primers (Table 19) to increase the reliability of results. Sequencing with both of the primers showed the insertion of Adenine nucleotide at the position NC_000023.11:g.44961373_44961374insA (Figure 15b). Together these results confirmed the successful knock-out of *KDM6A* in 5637 bladder cancer cell line.

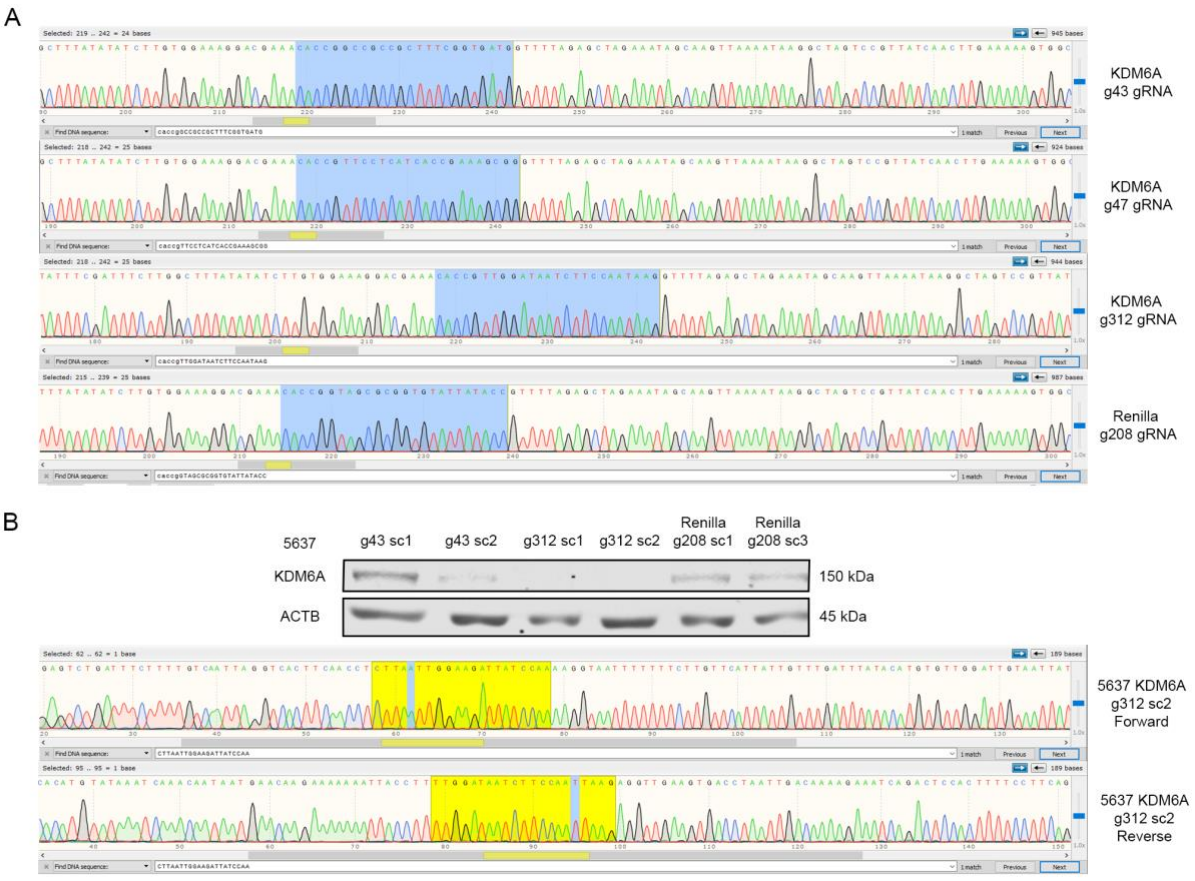


*Figure 15. Chromatogram images and protein levels of KDM6A knock-out via CRISPR-Cas9 method in 5637 bladder cancer cell line. (a) Sanger sequencing*

*results of three different KDM6A gRNAs and Renilla control gRNA (g43, g47, g312, g208) cloned into PX458 mammalian expression vector. Highlighted parts show gRNA sequences. Universal U6 promoter primer was used for sequencing. (b) (Upper panel) Western blot results of 5637 cell line grown as single colonies as a result of KDM6A CRISPR-Cas9 knock-out. ß-actin protein was used as internal control. (Lower panel) Sanger sequencing results of KDM6A knock-out colony that do not express KDM6A protein. Yellow highlighted section shows the part of the KDM6A reference sequence and the nucleotide highlighted with blue shows the insertion. Sequencing was applied to both strands of the DNA.*

#### *4.2.1.2. Effect of KDM6A knock-out on 5637 cell line viability*

To see the effect of KDM6A absence on 5637 bladder cancer cell line's proliferation we applied different cell viability assays to 5637 and KDM6A-null 5637 cells. According to the result of MTT proliferation assay (3 days), significantly decreased proliferation was seen in KDM6A-null cells (Figure 16a). However, cell counting assay that was carried on for 6 days and colony formation assay (12 days) have not shown any significant differences between 5637 and KDM6A-null 5637 cells' proliferation rates (Figure 16b,c). Considering all these results, although proliferation rates of 5637 and KDM6A-null 5637 differed in a short period of time, there were no significant difference over a long period of time.

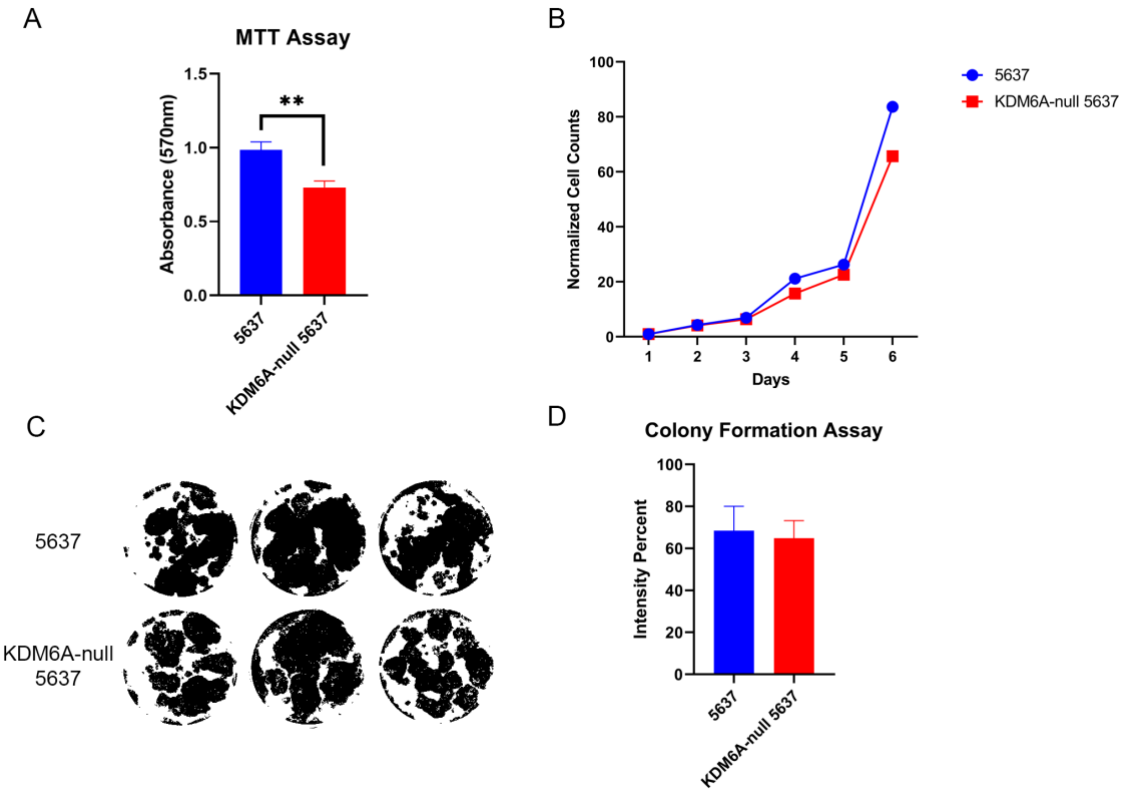


*Figure 16. Cell viability assays of 5637 and 5637 KDM6A-null cells. (a) Bar plot representation of MTT proliferation assay results comparing 5637 and KDM6A-null 5637 cells (Welch's t test p value = 0.0039) (*p < 0.05; **p < 0.01; ***p < 0.001). (b) Line graph representation of cell counting assay results for 6 days comparing 5637 and KDM6A-null 5637 cells. (c) (Left panel) Colony formation plate image of 5637 and 5637 KDM6A-null cells. (Right panel) Bar plot representation of colony formation assay signal intensity comparing 5637 and KDM6A-null 5637 cells (ns).*

#### *4.2.1.3. Chromatin level effect of KDM6A knock-out on 5637 cell line*

To see the effect of KDM6A absence on 5637 bladder cancer cell line at chromatin level, H3K4me3 chromatin immunoprecipitation (ChIP) was applied in both 5637 and KDM6A-null 5637 cells. Before sending the ChIP DNAs for

next generation sequencing, ChIP qPCR was applied to verify whether the ChIP experiment worked. Five different potential positive genes and two potential negative genes were selected according to our previous ChIP-Seq data. Selected positive genes; *EIF4B*, *RAB10*, *MCL1*, *DDIT4*, *TFAP2A*, *ATRAID* had higher % input IP values compared to negative genes; *PRAC1* and *GABRA2* as expected (Figure 17a). Unfortunately, sequencing quality of these ChIP samples were not as good as ChIP qPCR results. We were unable to analyze 5637 H3K4me3 ChIP-seq data properly because of its poor quality. However, KDM6A-null H3K4me3 ChIP-seq results were better compared to 5637 ChIP-seq results. Therefore, since we couldn't directly compare these two data, we focused on KDM6A-null H3K4me3 ChIP-seq data. After enrichment analysis, chromatin organization pathway was present among the most enriched Reactome (86) pathways (Figure 17b). When we further investigated the genes that are enriched in KDM6A-null 5637 cells and members of this pathway, some of the genes had increased peak signals in KDM6A-null cells compared to wild type 5637 cells including *HDAC1* and HMG20B (Figure 17c). However, these results need further validation as the quality of 5637 H3K4me3 ChIP-seq data is lower.

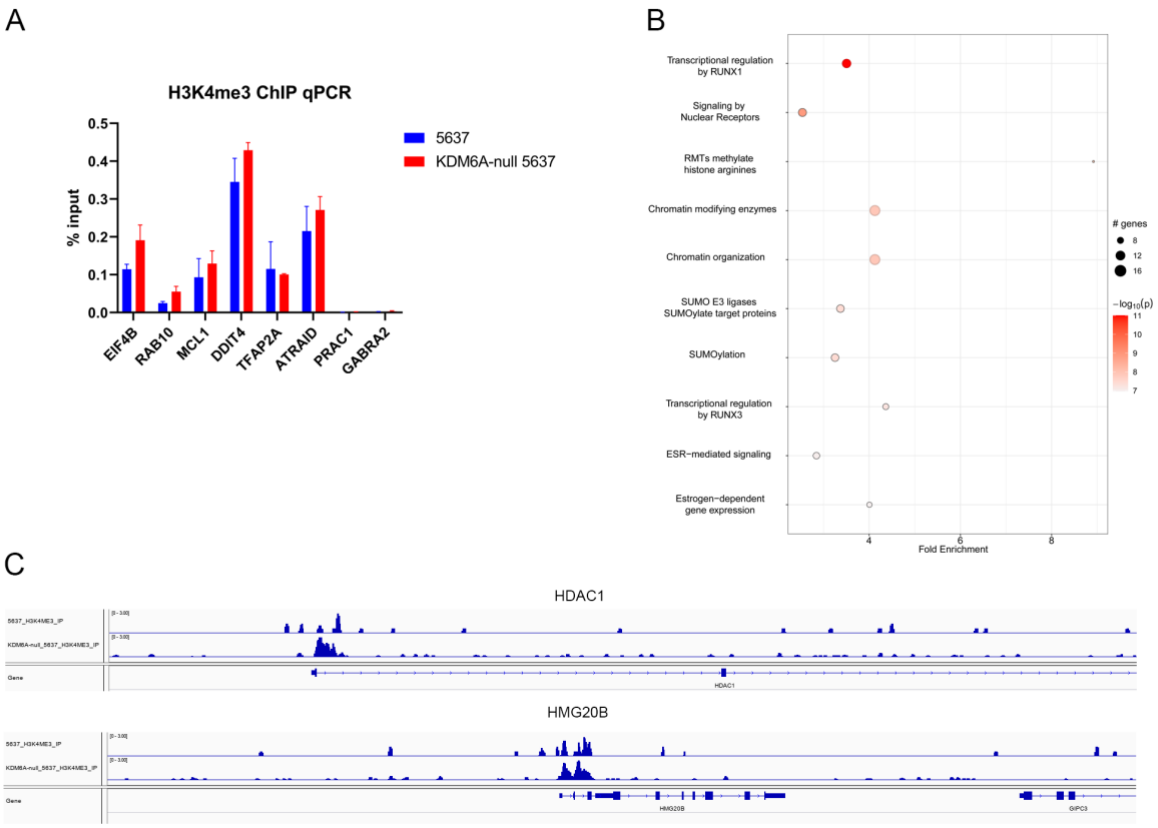


*Figure 17. Chromatin level effect of KDM6A knock-out. (a) qPCR results of H3K4me3 ChIP. % Input values of both 5637 and KDM6A-null 5637 cells. (b) Results of Reactome pathway enrichment analysis for the genes associated with top 500 H3K4me3 peaks in KDM6A-null 5637 cell line. Dot sizes indicating gene counts of specific terms. (c) IGV images showing the peaks located at the promoter regions of HDAC1 and HMG20B genes in both 5637 and KDM6A-null 5637 H3K4me3 ChIP-seq data.*

### *4.2.2. KDM6A-mutant 5637*

#### *4.2.2.1. Generating catalytically dead KDM6A containing lentiviral vector*

To generate KDM6A-mutant 5637 cells, complete *KDM6A* gene containing pCMV-HA-UTX mammalian expression vector was used. First, truncated Q555* point mutation was generated via PCR with the primers from Table 20. After that, truncated KDM6A was re-inserted in plasmid backbone. Quality of Sanger sequencing results of wild type and mutant *KDM6A* containing pCMV-HA-UTX plasmids were not good enough to speculate (Data not shown). To see the effect of the mutation on protein level, HEK293T cells were transfected with both mutant and wild type *KDM6A* containing plasmids. The sample that having the wild type *KDM6A* gene showed protein band at the expected size while the samples having mutant *KDM6A* did not show any bands at the size of wild type KDM6A. Instead, there were several bands around 65 kDa region for these samples (Figure 18a).

For permanent expression of mutant *KDM6A* gene, the Q555* mutated *KDM6A* gene insert was cloned into pUltra-hot lentiviral vector backbone. *KDM6A* insertion was validated from both ends with Sanger sequencing using two different primers. Both start position and the truncated end position of the mutant *KDM6A* were present in sequencing results (Figure 18b). Altogether, the results show the *KDM6A* Q555* truncating point mutation was generated properly.

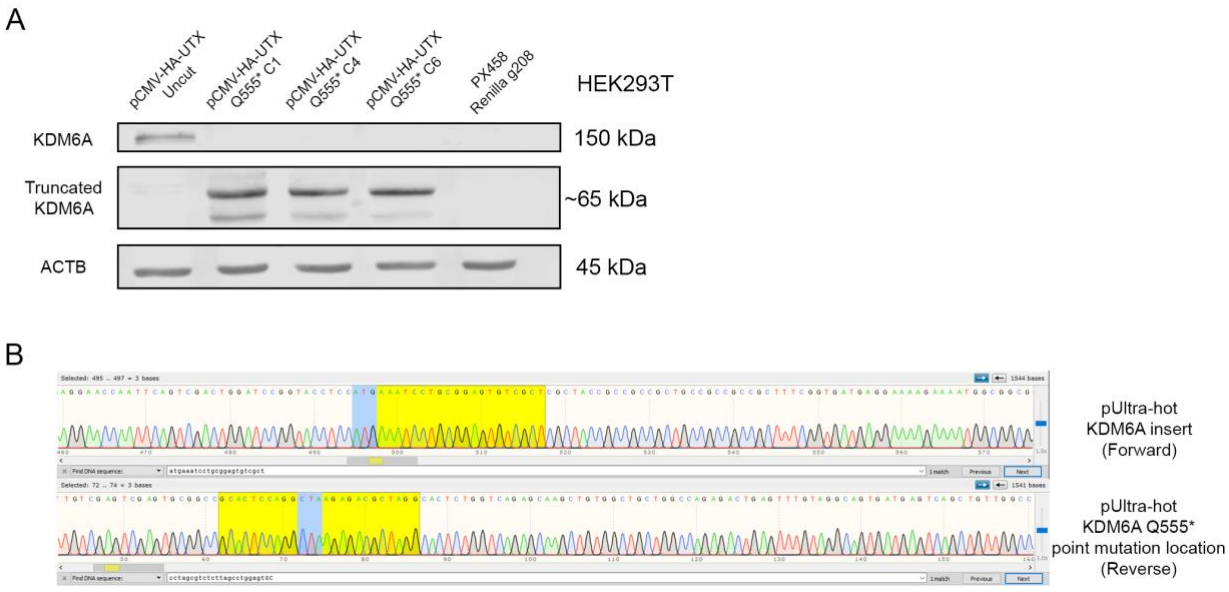


*Figure 18. Generation of KDM6A point mutation. (a) Western blot image of HEK293T transfected with KDM6A containing pCMV-HA-UTX plasmid. pCMV-HA-UTX Uncut sample contains wild type KDM6A gene while Q555* samples from different colonies contain mutated KDM6A. (b) Chromatogram images of mutated KDM6A inserted to pUltra-hot lentiviral vector. Upper image yellow highlighted region shows the beginning of the inserted KDM6A gene while blue highlighted part shows the start codon of the gene. Lower image yellow highlighted region shows the region of truncated mutation that causes the early stop codon UAG (blue highlight).*

## 5. DISCUSSION

Recently there have been several studies which aimed to identify the molecular subtypes of muscle invasive bladder cancer (MIBC) (4, 42). In this study we thoroughly re-analyzed MIBC ATAC-seq data (5) of 10 bladder cancer samples and identified three regulatory clusters. Since there were only 10 MIBC samples with available ATAC-seq data, the regulatory clusters we defined in this study may not be the final or definite but provided relevant regulatory characteristics of MIBC.

Our research, which focused specifically on the neuronal cluster we discovered, gave crucial information regarding the regulation of neuronal bladder cancer. Despite the fact that only one sample from the neuronal molecular subtype (4) had available ATAC-seq data, in-depth integration of our findings based on the neuronal regulatory regions we defined with gene expression and DNA methylation data from over 400 MIBC from the same TCGA cohort demonstrated the competence of the regulatory region definitions we constituted. (Figure 9). These findings highlight the use of regulatory genomics data in gaining a better understanding of the transcriptional networks that characterize tumor subtypes.

The neuronal regulatory cluster was, without a question, the most intriguing of the three regulatory clusters we identified. The WNT signaling pathway was shown to be the primary target of this cluster's target genes. The discovery of ß-catenin and TCF/LEF motifs enriched at neuronal regulatory elements, as well as the enrichment of ß-catenin mutations, concluded the circle explaining the molecular regulation of neuronal bladder cancer by WNT signaling. Within the context of the ß-catenin mutations we identified in bladder cancer, an exceptional enrichment for exon 3 ß-catenin mutations was remarkable. These mutations were previously reported as highly ‘oncogenic' (54, 87), disrupting β-catenin degradation and causing nuclear accumulation in the presence of phosphorylation site mutations S33, S37, and S45 (55, 88), which are the same mutations we discovered in neuronal bladder cancer. As a result, our findings and existing information strongly support the role of ß-catenin/WNT signaling in neuronal subtype.

We inquired about the function of WNT signaling in the ‘neuronal' character of this subtype after finding WNT signaling and ß-catenin mutations to be related with neuronal bladder cancer. WNT signaling modulates the self-renewal and differentiation of neural precursor cells, according to the literature (89, 90). Recent studies also showed that small molecules inducing WNT signaling enhance the neuronal differentiation of embryonic stem cells (91) and human urine cells can be converted to neurons using a combination of small molecules, including WNT activator (92). In our study, various genes involved in neurogenesis, including FGF9 and PROX1, appear to be among the target genes of neuronal regulatory elements that are also ß-catenin targets (Figure 11). These findings show that mutations in ß-catenin/ß-catenin destruction complex components cause aberrant activation of ß-catenin in neural bladder cancer, which activates WNT signaling and enhances neuronal differentiation.

Previously, it was also shown that expression of various WNT antagonists were increased in ß-catenin mutant hepatoblastomas (93) and murine lenses (94) indicating the activation of WNT signaling. In our analysis, identification of active neuronal regulatory elements targeting negative regulators of WNT signaling such as NKD1 and NOTUM, as well as considerably increased expression of these genes (Figure 12) suggests that ß-catenin mutations cause a similar effect in the neuronal subtype of bladder cancer.

According to the molecular subtypes defined in the latest TCGA study (4), neuronal subtype is the most aggressive one and it has the lowest survival rate among the other subtypes. Importantly, in the same TCGA study, 17 out of 20 samples belonging to the neuronal subtype did not reveal any neuroendocrine origin, indicating a convergence of molecular mechanisms in the development of regulatory signatures exclusive to this subtype. Despite the lowest survival rates, there are not yet available specific treatment options for neuronal bladder cancer.

The majority of current treatment options for bladder cancer are combine neoadjuvant chemotherapy with radical cystectomy or radiation (95). Thus, development of specific treatment methods for neuronal type bladder cancer is critical. Our findings strongly suggest that ß-catenin mutations activate WNT signaling in neuronal subtypes.

In addition, validation of our findings using gene expression data of two additional cohorts (58, 59) in addition to the TCGA cohort reinforces our findings on ß-catenin target gene activation in neuronal subtype bladder cancer. This hypothesis can be investigated using experimental methods, such as direct testing of the ß-catenin activation on solid tumor samples. Therefore, patients with neural bladder cancer may benefit greatly from the discovery of treatments that target ß-catenin. In fact, numerous therapies against ß-catenin or the components of the ß-catenin destruction complex have been developed and are in various phases of clinical trials for the treatment of colorectal cancer (96), pancreatic cancer, and numerous other solid tumors (97).

There have been several studies which showed the effect of KDM6A absence on certain cancer types. In one study, introduction of KDM6A in KDM6A-null urothelial carcinoma cell lines reduced long term growth, but not short-term growth (98). Another study showed that knockdown of KDM6A in urothelial cell lines can induce clonal cell population expansion (99). Correlatively, another study found out that in the presence of overactivated FGFR3, proliferation was increased in bladder cancer cells. However, introduction of *KDM6A* to KDM6A-null bladder cancer cell line UMUC1 removed the effect of FGFR3 on increased colony numbers and slightly decreased proliferation (100). Similarly, a different study showed that *KDM6A* knock-out in mice models led to tumor promotion in lung tumors (101). One study also showed that the loss of KDM6A enhanced the aggressive characteristics of human pancreatic ductal adenocarcinoma cell lines while overexpression of KDM6A showed the opposite effect (102). However, in our study we observed the opposite effect on 5637 bladder cancer cell line in short term growth (Figure 16a). Although KDM6A-null cells proliferation was decreased unexpectedly in short term, there were no significant changes in proliferation in long term growth (Figure 16b,c). These findings may indicate the distinct role of KDM6A other than its demethylase activity. In fact, one study suggested that KDM6A expression is associated with poor prognosis in NSCLC. They further suggested that KDM6A causes this by altering H3K4me3 levels by interacting with KMT2B independently of its main demethylase activity (28). Kim et al. also showed the similar activities of KDM6A in breast cancer (103). Overall, our findings on the

phenotypic effects of KDM6A knock-out in 5637 cells suggest no prominent effect on proliferation. In fact, another study showed that KDM6A knockdown in 5637 did not cause significant changes in proliferation but affected the migration and invasion characteristics of these cells (104). Thus, future work might be done to analyze the effects of KDM6A knock-out on invasion.

H3K4me3 ChIP sequencing results were not of the quality as we expected, although ChIP qPCR results were consistent. Based on the discussions with the center (GeneCore, EMBL) where ChIP-seq libraries were prepared and sequenced, the most likely cause for low sequencing quality might be attributed to the problems in library preparation, such that even re-sequencing of the same sequencing libraries did not make a major change in the quality of our ChIP-seq data. However, quality of KDM6A-null H3K4me3 ChIP-seq data had allowed us to interpret some information. We noticed the chromatin organization among the pathways that are enriched for the genes associated with KDM6A-null H3K4me3 peaks (Figure 17b). Some of the genes involved in 'chromatin organization' pathway had increased H3K4me3 signal at their promoter regions in KDM6A-null cells compared to KDM6A wild type cells. One such gene which is involved in chromatin organization was *HDAC1*. In a study, they showed contrasting role of HDAC1 and KDM6A during brown adipocyte differentiation *(105)*. In another study, authors showed increased HDAC1 levels as a result of KDM6A knock-down in murine mature T cells. They also pointed out the decreased H3K4me3 and H3K427ac active chromatin marks as a consequence of KDM6A knock-down (106). Although such an inference cannot be done directly for our results as the wild type 5637 data had poor quality, the information may provide important ideas for future search.

## 6. CONCLUSIONS AND FUTURE ASPECTS

In this thesis, active chromatin regions of muscle invasive bladder cancer were analyzed and integrated with DNA methylation and gene expression data. It has been revealed that damaging ß-catenin mutations are present in neuronal subtype of bladder cancer and these mutations are associated with WNT pathway activation in neuronal subtype. Therefore, targeting ß-catenin/Wnt pathway might be highly beneficial for the patients suffering from neuronal type of bladder cancer. In future studies, neuroendocrine differentiation will be modeled on normal bladder epithelial cells and treatments with various ß-catenin inhibitors will be applied to determine the effect of ß-catenin on neuroendocrine-like bladder cells.

The second aim of this thesis was to investigate the effects of the depletion of KDM6A chromatin modifier gene in bladder cancer cells. In this period of time, KDM6A knock-out cells were generated and the effect of KDM6A absence on their viability was investigated. But its effect on the chromatin level is not yet fully uncovered. In future studies, truncated KDM6A expressing bladder cancer cells will be generated with lentiviral transduction. Chromatin-level differences among wild type, truncated and null KDM6A expressing cells will be investigated.

## 7. REFERENCES


1. Bray F, Ferlay J, Soerjomataram I, Siegel RL, Torre LA, Jemal A. Global cancer statistics 2018: GLOBOCAN estimates of incidence and mortality worldwide for 36 cancers in 185 countries. CA Cancer J Clin. 2018;68(6):394-424.
2. Kamat AM, Hahn NM, Efstathiou JA, Lerner SP, Malmstrom PU, Choi W, et al. Bladder cancer. Lancet. 2016;388(10061):2796-810.
3. Ringuette-Goulet C, Bolduc S, Pouliot F. Modeling human bladder cancer. World J Urol. 2018;36(11):1759-66.
4. Robertson AG, Kim J, Al-Ahmadie H, Bellmunt J, Guo G, Cherniack AD, et al. Comprehensive Molecular Characterization of Muscle-Invasive Bladder Cancer. Cell. 2017;171(3):540-56 e25.
5. Corces MR, Granja JM, Shams S, Louie BH, Seoane JA, Zhou W, et al. The chromatin accessibility landscape of primary human cancers. Science. 2018;362(6413).
6. R Development Core Team. R: A language and environment for statistical computing. Vienna, Austria: R Foundation for Statistical Computing; 2020.
7. Hanahan D, Weinberg RA. The hallmarks of cancer. Cell. 2000;100(1):57-70.
8. Gordon JAR, Grandy, R.A., Lian, J.B., Stein, J.L., van Wijnen, A.J., Stein, G.S. Chromatin. In: Stanley Maloy KH, editor. Brenner's Encyclopedia of Genetics. Second Edition ed: Academic Press; 2013. p. 538-41.
9. Wei JW, Huang K, Yang C, Kang CS. Non-coding RNAs as regulators in epigenetics (Review). Oncol Rep. 2017;37(1):3-9.
10. Feinberg AP. The epigenetics of cancer etiology. Semin Cancer Biol. 2004;14(6):427-32.
11. Lund AH, van Lohuizen M. Epigenetics and cancer. Genes Dev. 2004;18(19):2315-35.
12. Martinez VG, Munera-Maravilla E, Bernardini A, Rubio C, Suarez-Cabrera C, Segovia C, et al. Epigenetics of Bladder Cancer: Where Biomarkers and Therapeutic Targets Meet. Front Genet. 2019;10:1125.

13. Suva ML, Riggi N, Bernstein BE. Epigenetic reprogramming in cancer. Science. 2013;339(6127):1567-70.
14. Portela A, Esteller M. Epigenetic modifications and human disease. Nat Biotechnol. 2010;28(10):1057-68.
15. Doane AS, Elemento O. Regulatory elements in molecular networks. Wiley Interdiscip Rev Syst Biol Med. 2017;9(3).
16. Lee BH, Rhie SK. Molecular and computational approaches to map regulatory elements in 3D chromatin structure. Epigenetics Chromatin. 2021;14(1):14.
17. Buenrostro JD, Giresi PG, Zaba LC, Chang HY, Greenleaf WJ. Transposition of native chromatin for fast and sensitive epigenomic profiling of open chromatin, DNA-binding proteins and nucleosome position. Nat Methods. 2013;10(12):1213-8.
18. Tran L, Xiao JF, Agarwal N, Duex JE, Theodorescu D. Advances in bladder cancer biology and therapy. Nat Rev Cancer. 2021;21(2):104-21.
19. Ler LD, Ghosh S, Chai X, Thike AA, Heng HL, Siew EY, et al. Loss of tumor suppressor KDM6A amplifies PRC2-regulated transcriptional repression in bladder cancer and can be targeted through inhibition of EZH2. Sci Transl Med. 2017;9(378).
20. van Haaften G, Dalgliesh GL, Davies H, Chen L, Bignell G, Greenman C, et al. Somatic mutations of the histone H3K27 demethylase gene UTX in human cancer. Nat Genet. 2009;41(5):521-3.
21. Kaneko S, Li X. X chromosome protects against bladder cancer in females via a KDM6A-dependent epigenetic mechanism. Sci Adv. 2018;4(6):eaar5598.
22. McLaughlin-Drubin ME, Munger K. Biochemical and functional interactions of human papillomavirus proteins with polycomb group proteins. Viruses. 2013;5(5):1231-49.
23. Park S, Kim GW, Kwon SH, Lee JS. Broad domains of histone H3 lysine 4 trimethylation in transcriptional regulation and disease. FEBS J. 2020;287(14):2891-902.
24. Zhao XD, Han X, Chew JL, Liu J, Chiu KP, Choo A, et al. Whole-genome mapping of histone H3 Lys4 and 27 trimethylations reveals distinct genomic compartments in human embryonic stem cells. Cell Stem Cell. 2007;1(3):286-98.

25. Hodl M, Basler K. Transcription in the absence of histone H3.2 and H3K4 methylation. Curr Biol. 2012;22(23):2253-7.
26. Benayoun BA, Pollina EA, Ucar D, Mahmoudi S, Karra K, Wong ED, et al. H3K4me3 breadth is linked to cell identity and transcriptional consistency. Cell. 2014;158(3):673-88.
27. Chen K, Chen Z, Wu D, Zhang L, Lin X, Su J, et al. Broad H3K4me3 is associated with increased transcription elongation and enhancer activity at tumor-suppressor genes. Nat Genet. 2015;47(10):1149-57.
28. Leng X, Wang J, An N, Wang X, Sun Y, Chen Z. Histone 3 lysine-27 demethylase KDM6A coordinates with KMT2B to play an oncogenic role in NSCLC by regulating H3K4me3. Oncogene. 2020;39(41):6468-79.
29. Beyaz S, Kim JH, Pinello L, Xifaras ME, Hu Y, Huang J, et al. The histone demethylase UTX regulates the lineage-specific epigenetic program of invariant natural killer T cells. Nat Immunol. 2017;18(2):184-95.
30. Cottone L, Cribbs AP, Khandelwal G, Wells G, Ligammari L, Philpott M, et al. Inhibition of Histone H3K27 Demethylases Inactivates Brachyury (TBXT) and Promotes Chordoma Cell Death. Cancer Res. 2020;80(20):4540-51.
31. Richters A, Aben KKH, Kiemeney L. The global burden of urinary bladder cancer: an update. World J Urol. 2020;38(8):1895-904.
32. Cumberbatch MG, Rota M, Catto JW, La Vecchia C. The Role of Tobacco Smoke in Bladder and Kidney Carcinogenesis: A Comparison of Exposures and Meta-analysis of Incidence and Mortality Risks. Eur Urol. 2016;70(3):458-66.
33. Shariat SF, Sfakianos JP, Droller MJ, Karakiewicz PI, Meryn S, Bochner BH. The effect of age and gender on bladder cancer: a critical review of the literature. BJU Int. 2010;105(3):300-8.
34. Lenis AT, Lec PM, Chamie K, Mshs MD. Bladder Cancer: A Review. JAMA. 2020;324(19):1980-91.
35. Necchi A, Anichini A, Raggi D, Briganti A, Massa S, Luciano R, et al. Pembrolizumab as Neoadjuvant Therapy Before Radical Cystectomy in Patients With

Muscle-Invasive Urothelial Bladder Carcinoma (PURE-01): An Open-Label, Single-Arm, Phase II Study. J Clin Oncol. 2018;36(34):3353-60.
36. Fong MHY, Feng M, McConkey DJ, Choi W. Update on bladder cancer molecular subtypes. Transl Androl Urol. 2020;9(6):2881-9.
37. Blaveri E, Simko JP, Korkola JE, Brewer JL, Baehner F, Mehta K, et al. Bladder cancer outcome and subtype classification by gene expression. Clin Cancer Res. 2005;11(11):4044-55.
38. Choi W, Porten S, Kim S, Willis D, Plimack ER, Hoffman-Censits J, et al. Identification of distinct basal and luminal subtypes of muscle-invasive bladder cancer with different sensitivities to frontline chemotherapy. Cancer Cell. 2014;25(2):152-65.
39. Hedegaard J, Lamy P, Nordentoft I, Algaba F, Hoyer S, Ulhoi BP, et al. Comprehensive Transcriptional Analysis of Early-Stage Urothelial Carcinoma. Cancer Cell. 2016;30(1):27-42.
40. Sjodahl G, Lovgren K, Lauss M, Patschan O, Gudjonsson S, Chebil G, et al. Toward a molecular pathologic classification of urothelial carcinoma. Am J Pathol. 2013;183(3):681-91.
41. Cancer Genome Atlas Research N. Comprehensive molecular characterization of urothelial bladder carcinoma. Nature. 2014;507(7492):315-22.
42. Kamoun A, de Reynies A, Allory Y, Sjodahl G, Robertson AG, Seiler R, et al. A Consensus Molecular Classification of Muscle-invasive Bladder Cancer. Eur Urol. 2020;77(4):420-33.
43. Lindskrog SV, Prip F, Lamy P, Taber A, Groeneveld CS, Birkenkamp-Demtroder K, et al. An integrated multi-omics analysis identifies prognostic molecular subtypes of non-muscle-invasive bladder cancer. Nat Commun. 2021;12(1):2301.
44. Gui Y, Guo G, Huang Y, Hu X, Tang A, Gao S, et al. Frequent mutations of chromatin remodeling genes in transitional cell carcinoma of the bladder. Nat Genet. 2011;43(9):875-8.
45. Ozgun G, Senturk S, Erkek-Ozhan S. Retinoic acid signaling and bladder cancer: Epigenetic deregulation, therapy and beyond. Int J Cancer. 2020.

46. Sanchez-Carbayo M. Hypermethylation in bladder cancer: biological pathways and translational applications. Tumour Biol. 2012;33(2):347-61.
47. Zhang Y, Wang X. Targeting the Wnt/beta-catenin signaling pathway in cancer. J Hematol Oncol. 2020;13(1):165.
48. Ge X, Wang X. Role of Wnt canonical pathway in hematological malignancies. J Hematol Oncol. 2010;3:33.
49. Gajos-Michniewicz A, Czyz M. WNT Signaling in Melanoma. Int J Mol Sci. 2020;21(14).
50. He S, Tang S. WNT/beta-catenin signaling in the development of liver cancers. Biomed Pharmacother. 2020;132:110851.
51. Azbazdar Y, Karabicici M, Erdal E, Ozhan G. Regulation of Wnt Signaling Pathways at the Plasma Membrane and Their Misregulation in Cancer. Front Cell Dev Biol. 2021;9:631623.
52. Bugter JM, Fenderico N, Maurice MM. Mutations and mechanisms of WNT pathway tumour suppressors in cancer. Nat Rev Cancer. 2021;21(1):5-21.
53. Kim S, Jeong S. Mutation Hotspots in the beta-Catenin Gene: Lessons from the Human Cancer Genome Databases. Mol Cells. 2019;42(1):8-16.
54. Gao C, Wang Y, Broaddus R, Sun L, Xue F, Zhang W. Exon 3 mutations of CTNNB1 drive tumorigenesis: a review. Oncotarget. 2018;9(4):5492-508.
55. Amit S, Hatzubai A, Birman Y, Andersen JS, Ben-Shushan E, Mann M, et al. Axin-mediated CKI phosphorylation of beta-catenin at Ser 45: a molecular switch for the Wnt pathway. Genes Dev. 2002;16(9):1066-76.
56. Fujimori M, Ikeda S, Shimizu Y, Okajima M, Asahara T. Accumulation of beta-catenin protein and mutations in exon 3 of beta-catenin gene in gastrointestinal carcinoid tumor. Cancer Res. 2001;61(18):6656-9.
57. Weber M, Hellmann I, Stadler MB, Ramos L, Paabo S, Rebhan M, et al. Distribution, silencing potential and evolutionary impact of promoter DNA methylation in the human genome. Nat Genet. 2007;39(4):457-66.

58. Sjodahl G, Eriksson P, Liedberg F, Hoglund M. Molecular classification of urothelial carcinoma: global mRNA classification versus tumour-cell phenotype classification. J Pathol. 2017;242(1):113-25.
59. Iyer G, Al-Ahmadie H, Schultz N, Hanrahan AJ, Ostrovnaya I, Balar AV, et al. Prevalence and co-occurrence of actionable genomic alterations in high-grade bladder cancer. J Clin Oncol. 2013;31(25):3133-40.
60. Ewels PA, Peltzer A, Fillinger S, Patel H, Alneberg J, Wilm A, et al. The nf-core framework for community-curated bioinformatics pipelines. Nat Biotechnol. 2020;38(3):276-8.
61. Zhang Y, Liu T, Meyer CA, Eeckhoute J, Johnson DS, Bernstein BE, et al. Model-based analysis of ChIP-Seq (MACS). Genome Biol. 2008;9(9):R137.
62. Ulgen E, Ozisik O, Sezerman OU. pathfindR: An R Package for Comprehensive Identification of Enriched Pathways in Omics Data Through Active Subnetworks. Front Genet. 2019;10:858.
63. Frankish A, Diekhans M, Ferreira AM, Johnson R, Jungreis I, Loveland J, et al. GENCODE reference annotation for the human and mouse genomes. Nucleic Acids Res. 2019;47(D1):D766-D73.
64. Yu G, Wang LG, Han Y, He QY. clusterProfiler: an R package for comparing biological themes among gene clusters. OMICS. 2012;16(5):284-7.
65. Chen EY, Tan CM, Kou Y, Duan Q, Wang Z, Meirelles GV, et al. Enrichr: interactive and collaborative HTML5 gene list enrichment analysis tool. BMC Bioinformatics. 2013;14:128.
66. Kuleshov MV, Jones MR, Rouillard AD, Fernandez NF, Duan Q, Wang Z, et al. Enrichr: a comprehensive gene set enrichment analysis web server 2016 update. Nucleic Acids Res. 2016;44(W1):W90-7.
67. Heinz S, Benner C, Spann N, Bertolino E, Lin YC, Laslo P, et al. Simple combinations of lineage-determining transcription factors prime cis-regulatory elements required for macrophage and B cell identities. Mol Cell. 2010;38(4):576-89.
68. Kolde R. Pheatmap: pretty heatmaps. R package version. 2012;61:617.

69. Yu G. enrichplot: Visualization of Functional Enrichment Result. R package version 1.4.0. 2019.
70. Goldman M, Craft B, Hastie M, Repečka K, McDade F, Kamath A, et al. The UCSC Xena platform for public and private cancer genomics data visualization and interpretation. bioRxiv. 2019:326470.
71. Signorell A. DescTools: Tools for Descriptive Statistics. 2020.
72. Corradin O, Saiakhova A, Akhtar-Zaidi B, Myeroff L, Willis J, Cowper-Sal lari R, et al. Combinatorial effects of multiple enhancer variants in linkage disequilibrium dictate levels of gene expression to confer susceptibility to common traits. Genome Res. 2014;24(1):1-13.
73. Yao L, Shen H, Laird PW, Farnham PJ, Berman BP. Inferring regulatory element landscapes and transcription factor networks from cancer methylomes. Genome Biol. 2015;16:105.
74. Schmidt-Ott KM, Masckauchan TNH, Chen X, Hirsh BJ, Sarkar A, Yang J, et al. β-catenin/TCF/Lef controls a differentiation-associated transcriptional program in renal epithelial progenitors. Development. 2007;134(17):3177-90.
75. Shimizu T, Kagawa T, Inoue T, Nonaka A, Takada S, Aburatani H, et al. Stabilized beta-catenin functions through TCF/LEF proteins and the Notch/RBP-Jkappa complex to promote proliferation and suppress differentiation of neural precursor cells. Mol Cell Biol. 2008;28(24):7427-41.
76. Miravet S, Piedra J, Miro F, Itarte E, Garcia de Herreros A, Dunach M. The transcriptional factor Tcf-4 contains different binding sites for beta-catenin and plakoglobin. J Biol Chem. 2002;277(3):1884-91.
77. Ou CY, LaBonte MJ, Manegold PC, So AY, Ianculescu I, Gerke DS, et al. A coactivator role of CARM1 in the dysregulation of beta-catenin activity in colorectal cancer cell growth and gene expression. Mol Cancer Res. 2011;9(5):660-70.
78. Stancikova J, Krausova M, Kolar M, Fafilek B, Svec J, Sedlacek R, et al. NKD1 marks intestinal and liver tumors linked to aberrant Wnt signaling. Cell Signal. 2015;27(2):245-56.

79. Martynoga B, Drechsel D, Guillemot F. Molecular control of neurogenesis: a view from the mammalian cerebral cortex. Cold Spring Harb Perspect Biol. 2012;4(10).
80. Yusuf IO, Cheng PH, Chen HM, Chang YF, Chang CY, Yang HI, et al. Fibroblast Growth Factor 9 Suppresses Striatal Cell Death Dominantly Through ERK Signaling in Huntington's Disease. Cell Physiol Biochem. 2018;48(2):605-17.
81. Mrozik KM, Blaschuk OW, Cheong CM, Zannettino ACW, Vandyke K. N-cadherin in cancer metastasis, its emerging role in haematological malignancies and potential as a therapeutic target in cancer. BMC Cancer. 2018;18(1):939.
82. Plissonnier ML, Fauconnet S, Bittard H, Lascombe I. The antidiabetic drug ciglitazone induces high grade bladder cancer cells apoptosis through the up-regulation of TRAIL. PLoS One. 2011;6(12):e28354.
83. Heuberger J, Birchmeier W. Interplay of cadherin-mediated cell adhesion and canonical Wnt signaling. Cold Spring Harb Perspect Biol. 2010;2(2):a002915.
84. Shang S, Hua F, Hu ZW. The regulation of beta-catenin activity and function in cancer: therapeutic opportunities. Oncotarget. 2017;8(20):33972-89.
85. Tate JG, Bamford S, Jubb HC, Sondka Z, Beare DM, Bindal N, et al. COSMIC: the Catalogue Of Somatic Mutations In Cancer. Nucleic Acids Res. 2019;47(D1):D941-D7.
86. Jassal B, Matthews L, Viteri G, Gong C, Lorente P, Fabregat A, et al. The reactome pathway knowledgebase. Nucleic Acids Res. 2020;48(D1):D498-D503.
87. Liu Y, Patel L, Mills GB, Lu KH, Sood AK, Ding L, et al. Clinical significance of CTNNB1 mutation and Wnt pathway activation in endometrioid endometrial carcinoma. J Natl Cancer Inst. 2014;106(9).
88. Liu C, Li Y, Semenov M, Han C, Baeg GH, Tan Y, et al. Control of beta-catenin phosphorylation/degradation by a dual-kinase mechanism. Cell. 2002;108(6):837-47.
89. Inestrosa NC, Varela-Nallar L. Wnt signaling in the nervous system and in Alzheimer's disease. J Mol Cell Biol. 2014;6(1):64-74.
90. Inestrosa NC, Varela-Nallar L. Wnt signalling in neuronal differentiation and development. Cell Tissue Res. 2015;359(1):215-23.

91. Davidson KC, Jamshidi P, Daly R, Hearn MT, Pera MF, Dottori M. Wnt3a regulates survival, expansion, and maintenance of neural progenitors derived from human embryonic stem cells. Mol Cell Neurosci. 2007;36(3):408-15.
92. Xu G, Wu F, Gu X, Zhang J, You K, Chen Y, et al. Direct Conversion of Human Urine Cells to Neurons by Small Molecules. Sci Rep. 2019;9(1):16707.
93. Koch A, Waha A, Hartmann W, Hrychyk A, Schuller U, Waha A, et al. Elevated expression of Wnt antagonists is a common event in hepatoblastomas. Clin Cancer Res. 2005;11(12):4295-304.
94. Martinez G, Wijesinghe M, Turner K, Abud HE, Taketo MM, Noda T, et al. Conditional mutations of beta-catenin and APC reveal roles for canonical Wnt signaling in lens differentiation. Invest Ophthalmol Vis Sci. 2009;50(10):4794-806.
95. Batista da Costa J, Gibb EA, Bivalacqua TJ, Liu Y, Oo HZ, Miyamoto DT, et al. Molecular Characterization of Neuroendocrine-like Bladder Cancer. Clin Cancer Res. 2019;25(13):3908-20.
96. Cheng X, Xu X, Chen D, Zhao F, Wang W. Therapeutic potential of targeting the Wnt/beta-catenin signaling pathway in colorectal cancer. Biomed Pharmacother. 2019;110:473-81.
97. Jung YS, Park JI. Wnt signaling in cancer: therapeutic targeting of Wnt signaling beyond beta-catenin and the destruction complex. Exp Mol Med. 2020;52(2):183-91.
98. Lang A, Yilmaz M, Hader C, Murday S, Kunz X, Wagner N, et al. Contingencies of UTX/KDM6A Action in Urothelial Carcinoma. Cancers (Basel). 2019;11(4).
99. Lang A, Whongsiri P, Yilmaz M, Lautwein T, Petzsch P, Greife A, et al. Knockdown of UTX/KDM6A Enriches Precursor Cell Populations in Urothelial Cell Cultures and Cell Lines. Cancers (Basel). 2020;12(4).
100. Barrows D, Feng L, Carroll TS, Allis CD. Loss of UTX/KDM6A and the activation of FGFR3 converge to regulate differentiation gene-expression programs in bladder cancer. Proc Natl Acad Sci U S A. 2020;117(41):25732-41.
101. Wu Q, Tian Y, Zhang J, Tong X, Huang H, Li S, et al. In vivo CRISPR screening unveils histone demethylase UTX as an important epigenetic regulator in lung tumorigenesis. Proc Natl Acad Sci U S A. 2018;115(17):E3978-E86.

102. Watanabe S, Shimada S, Akiyama Y, Ishikawa Y, Ogura T, Ogawa K, et al. Loss of KDM6A characterizes a poor prognostic subtype of human pancreatic cancer and potentiates HDAC inhibitor lethality. Int J Cancer. 2019;145(1):192-205.
103. Kim JH, Sharma A, Dhar SS, Lee SH, Gu B, Chan CH, et al. UTX and MLL4 coordinately regulate transcriptional programs for cell proliferation and invasiveness in breast cancer cells. Cancer Res. 2014;74(6):1705-17.
104. Liu L, Cui J, Zhao Y, Liu X, Chen L, Xia Y, et al. KDM6A-ARHGDIB axis blocks metastasis of bladder cancer by inhibiting Rac1. Mol Cancer. 2021;20(1):77.
105. Li F, Wu R, Cui X, Zha L, Yu L, Shi H, et al. Histone Deacetylase 1 (HDAC1) Negatively Regulates Thermogenic Program in Brown Adipocytes via Coordinated Regulation of Histone H3 Lysine 27 (H3K27) Deacetylation and Methylation. J Biol Chem. 2016;291(9):4523-36.
106. Oswald F, Rodriguez P, Giaimo BD, Antonello ZA, Mira L, Mittler G, et al. A phospho-dependent mechanism involving NCoR and KMT2D controls a permissive chromatin state at Notch target genes. Nucleic Acids Res. 2016;44(10):4703-20.

# 8. APPENDIX

## 8.1. Research Ethics Committee Approval

**İZMİR BİYOTIP VE GENOM MERKEZİ**
**GİRİŞİMSEL OLMAYAN ARAŞTIRMALAR ETİK KURULU (İBG-GOEK)**
**KARARI**

| | | | |
|---|---|---|---|
| **Toplantı Tarihi** | : 16/05/2020 | **Toplantı Günü** | : Cumartesi |
| **Toplantı Sayısı** | : 6 | **Toplantı Saati** | : 13:00 |

**Sayın Gökhan KARAKÜLAH,**

**2020-018 Protokol No'lu;** sorumlusu olduğunuz "Mesane tümör oluşumunda görev alan moleküler mekanizmaların deneysel ve hesaplamalı yaklaşımlar ile anlaşılması" başlıklı araştırmanın uygulanmasında etik açıdan sakınca olmadığına oy birliği ile karar verilmiştir.

Bilgilerinizi ve gereğini rica ederiz.

Pandemi süresince online ortamda gerçekleştirilen toplantımızda alınan kararlar tek imzalı olarak düzenlenmektedir. Pandemi sona erdikten sonra ıslak imzalı karar belgesi teslim edilecektir.

# ALEYNA ERAY

## Personal Information

### Contact Information

Contact Address

Telephone

Email

Web Page

### Education Information

03 August 2018 - Now (3 Year 1 Month)
Yüksek Lisans, Tezli Program, DOKUZ EYLÜL ÜNİVERSİTESİ, TÜRKİYE
İZMİR ULUSLARARASI BİYOTIP VE GENOM ENSTİTÜSÜ, MOLEKÜLER BİYOLOJİ VE GENETİK (YL) (TEZLİ) (İNGİLİZCE)
Cumulative Grade Point Average: 3.81 / 4.0

03 September 2014 - 30 May 2018 (3 Year 9 Month)
Lisans, Anadal/Normal Öğretim, ULUDAĞ ÜNİVERSİTESİ, TÜRKİYE
FEN-EDEBİYAT FAKÜLTESİ, MOLEKÜLER BİYOLOJİ VE GENETİK PR.
Diploma Number: 2018-16977
Cumulative Grade Point Average: 3.58 / 4.0

### Foreign Language Information

İNGİLİZCE (Reading: İyi, Writing: İyi, Speaking: İyi)

## R&D Competency

### Articles

A. ERAY, P. Y. GUENERİ, G. O. YİLMAZ, G. KARAKUELAH & S. ERKEK-OZHAN, Analysis of open chromatin regions in bladder cancer links beta-catenin mutations and Wnt signaling with neuronal subtype of bladder cancer, SCIENTIFIC REPORTS, 2020, 2045-2322, 10, 1.

### Conference Papers

A. ERAY, P. Y. GÜNERİ SÖZERİ, G. ÖZDEN YILMAZ, G. KARAKÜLAH & S. ERKEK ÖZHAN, Analysis of ATAC-Seq data for bladder cancer reveals the link between WNT pathway ß-catenin mutations and neuronal subtype of bladder cancer, Poster Sunumu, EMBL Chromatin and Epigenetics, 17 May 2021, 20 May 2021.

P. Y. GÜNERİ SÖZERİ, G. ÖZDEN YILMAZ, A. ERAY, S. N. ATABEY, Ş. ŞENTÜRK & S. ERKEK ÖZHAN, İNVAZIV OLAN VE INVAZIV OLMAYAN MESANE KANSERI HÜCRE HATLARINI KARAKTERIZE EDEN TRANSKRIPSIYONEL DÜZENLEYICI AĞLARIN TANIMLANMASI, Sözlü Sunum, Onkolojide İz Bırakanlar Zirvesi, 14 November 2019, 17 November 2019, 38 - 38.

A. ERAY, G. ÖZDEN YILMAZ, P. Y. GÜNERİ SÖZERİ & S. ERKEK ÖZHAN, İdrardan elde edilen ürotelyal kök hücreler ile mesane kanserinin epigenetik regülasyonunun belirlenmesi, Sözlü Sunum, Onkolojide İz Bırakanlar Zirvesi, 14 November 2019, 17 November 2019, 37 - 37.

P. Y. GÜNERİ SÖZERİ, G. ÖZDEN YILMAZ, A. ERAY, S. N. ATABEY, Ş. ŞENTÜRK & S. ERKEK ÖZHAN, Identification of transcriptional regulatory networks characterizing invasive and non-invasive bladder cancer cell lines, Poster Sunumu, The International Symposium on Health Informatics and Bioinformatics (HIBIT), 17 October 2019, 18 October 2019.

P. Y. GÜNERİ SÖZERİ, G. ÖZDEN YILMAZ, A. ERAY, S. N. ATABEY, Ş. ŞENTÜRK & S. ERKEK ÖZHAN, Identification of transcriptional regulatory networks characterizing invasive and non-invasive bladder cancer cell lines, Sözlü Sunum, International Bladder Cancer Network Annual Meeting, 2019, 03 October 2019, 05 October 2019.

P. Y. GÜNERİ SÖZERİ, G. ÖZDEN YILMAZ, A. ERAY, S. N. ATABEY, Ş. ŞENTÜRK & S. ERKEK ÖZHAN, Identification of transcriptional regulatory networks characterizing invasive and non-invasive bladder cancer cell lines, Poster Sunumu, EMBO Young Scientists Forum 2019, 27 June 2019, 28 June 2019.

A. ERAY, G. ÖZDEN YILMAZ, P. Y. GÜNERİ SÖZERİ & S. ERKEK ÖZHAN, Pan-cancer analysis of UTX and MLL3 mutations in gene regulation, Poster Sunumu, 11th EMBO Young Scientists Forum , 27 June 2019, 28 June 2019.

## TÜBİTAK Scholarships and Fundings

**BIDEB Supports**

ALEYNA ERAY, Etkinlik Destekleri ve Eğitim Bursları Müdürlüğü, 2210-A Genel Yurt İçi Yüksek Lisans Burs Programı, Başvurusu Reddedildi, 2018 - 2, 10/1/18 - 9/30/20.
ALEYNA ERAY, Etkinlik Destekleri ve Eğitim Bursları Müdürlüğü, 2210-A Genel Yurt İçi Yüksek Lisans Burs Programı, Başvurusu Reddedildi, 2019 - 2, 10/1/19 - 9/30/21.

**Number of Panelist/Observer/Reporter Jobs**

| | | | |
|---|---|---|---|
| Refereeing/Panelist/Outer Consultant Count | ARDEB/BİDEB 0 | TEYDEB 0 | Total 0 |
| Number of Observer/Consultant Jobs | ARDEB/BİDEB 0 | TEYDEB 0 | Total 0 |
| Number of Reporter Jobs | ARDEB/BİDEB 0 | TEYDEB 0 | Total 0 |